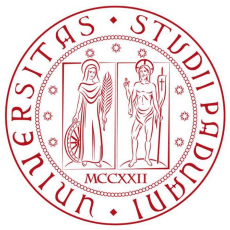

UNIVERSITÀ DEGLI STUDI DI PADOVA

Dipartimento di Fisica e Astronomia "Galileo Galilei"

Corso di Laurea Triennale in Fisica

Tesi di Laurea

Squeezed states of light to enhance the sensitivity of axion detectors

Relatore

Prof. Jean-Pierre Zendri

Correlatore

Dr. Antonello Ortolan

Laureando

Benedetta Rosatello

Anno Accademico 2021/2022

Contents

Abstract

Haloscope's sensitivity is limited by the quantum features of microwave radiation employed to detect axion cold dark matter signals. So far, many experiments have approached the edge called *standard quantum limit* (SQL). An article published lately on *Nature* [1] discusses how the HAYSTAC experiment (*Haloscope at Yale Sensitive to Axion Cold dark matter*) managed to overcome the SQL by using quantum states of electromagnetic radiation, the so-called *squeezed states*.
In the present thesis the aforementioned experiment will be studied. The reasons for searching for the QCD axion and other axion-like particles (ALPs) will be introduced, as well as the mode of operation of the main axion detectors. Then, it will be studied the SQL of classical signal amplifiers and how it can be overcome by using the *phase-sensitive* amplification of the *Josephson Parametric Amplifiers* to produce microwave squeezing. Finally, the HAYSTAC experimental setup will be discussed as well as its up-to-date results and how the detector can be enhanced further in future.

La sensibilità dei rivelatori haloscopici di materia oscura assionica è limitata dalle proprietà quantistiche della radiazione a microonde usata per la rivelazione. Attualmente molti rivelatori operano vicino a questo limite quantistico standard *(SQL). In un recente articolo apparso sulla rivista* Nature *[1] è stato riportato come impiegando stati non classici della radiazione elettromagnetica chiamati* stati squeezed *è stato possibile superare lo SQL presso l'esperimento HAYSTAC (*Haloscope at Yale Sensitive to Axion Cold dark matter*).*
Il presente lavoro di tesi consiste nell'analisi dell'esperimento citato. Inizialmente verranno introdotte le motivazioni per la ricerca di assioni QCD e di altre particelle di tipo assionico (ALPs), oltre al principio di funzionamento dei principali rivelatori assionici. Successivamente si analizzerà la natura dello SQL legata all'amplificazione dei segnali, si vedrà come gli attuali limiti possono essere superati utilizzando stati squeezed e si mostrerà come tali stati siano realizzabili tramite un'amplificazione phase-sensitive *ottenuta mediante l'impiego dei* Josephson Parametric Amplifiers. *Infine, saranno illustrati il setup sperimentale di HAYSTAC e i risultati ottenuti, nonché le sue potenzialità future.*

Chapter 1

Introduction to light dark matter

The Standard Model of Particle Physics (SM) is a quantum field theory describing quarks and leptons constituting matter as well as their interactions (electromagnetic, weak and strong). Despite the great accuracy of its predictions and the experimental verification of many of them, the SM has some unresolved issues. Among them, the so-called *strong CP problem* and the nature of *cold dark matter* entail the introduction of a new hypothetical particle beyond the SM: the *Quantum Chromodynamics (QCD) axion.*

The CP symmetry is the combination of charge conjugation (C) with parity reversal (P); violations of this symmetry have been observed in laboratories for processes generated by the weak interaction which is responsible for radioactive decays. As regards the strong interaction, a neutron electric dipole moment (nEDM) would violate the CP symmetry: the neutron is the subatomic particle made up of two quarks down and one quark up with electrical charges $-1/3\,e$ and $+2/3\,e$ respectively, bound together by the strong force. If present, a nEDM would receive a contribution from the strong and weak interactions and it would be proportional to the total CP-violating angle $\overline{\theta}$ [2]:

$$|\mathbf{d}| \simeq 3.6 \times 10^{-16}\ \overline{\theta}\ e \cdot cm. \tag{1.1}$$

The latest searches have put an upper limit for the neutron EDM, $|\mathbf{d}| < 1.8 \times 10^{-26}\ e \cdot cm$ [3], hence

$$\overline{\theta} < 5 \times 10^{-11}. \tag{1.2}$$

Such a small value for the total CP-violating angle may be the consequence of a very precise cancellation between the unrelated CP-violating parameters of two fundamental interactions, suggesting some missing fundamental physics underlying the strong force.

In order to explain this limit for $\overline{\theta}$, in 1977 Roberto Peccei and Helen Quinn [4] proposed a model in which they promoted it to a dynamical quantity proportional to the new field, $\overline{\theta} \propto a(t,x)$, a pseudoscalar (it changes its sign under a P transformation) bosonic field permeating all space and to which is associated, according to quantum mechanics, a new particle beyond the SM: the QCD axion. This field would oscillate around the minimum of the potential which would be energetically favorable, hence setting the total nEDM close to zero.
To add the QCD axion to the SM, the Peccei-Quinn global chiral U(1) symmetry was introduced (the symmetry transformation $\Phi \to \Phi' = e^{-i\alpha}\Phi$ is constant in space and time and acts differently on left-handed and right-handed particles). The $U(1)_{PQ}$ symmetry would have undergone a spontaneous symmetry breaking at a certain temperature T_{PQ} before or after the hot Big Bang phase when the temperature of the early universe was at its maximum, T_{hot}. In both scenarios, as the universe slowed down to an an expansion rate below the natural frequency ν_a (such that $E = h\nu_a = m_a c^2$ where m_a is the rest mass of the axion), the axion field begun to oscillate and the number of axion particles grew. The QCD axion's mass can be estimated considering its analogies with the neutral pion, which leads to the relation $m_a f_a \simeq m_\pi f_\pi$ where f_a is a parameter proportional to the energy of the spontaneous $U(1)_{PQ}$ symmetry breaking. Knowing the experimental measurement for the pion's mass m_π and

the value of the constant f_π from the pion's rate of decay (generated by the weak interaction), it is possible to estimate [5]:

$$m_a = 5.691(51)\ \mu eV \left(\frac{10^{12} GeV}{f_a}\right). \tag{1.3}$$

Some cosmological scenarios suggest that the QCD axion or other suitable *axion like particles* (*ALPs*) are good candidates for providing cold dark matter. It is worth noticing that ALPs can be described by two independent parameters (m_a,f_a) of a pseudoscalar boson emerging from spontaneously broken global chiral symmetry [6].
The presence of dark matter was first proposed by Fritz Zwicky in 1930's to explain the cluster of galaxies: these are structures of thousands of galaxies bound together by gravity. Studying the Coma Cluster, Zwicky [7] found that in order to keep the cluster together, it was required a much higher mass than that of the observed galaxies and theorised the presence of a big amount of dark matter. Many astronomical observations of clustering of galaxies and of their gravitational lensing effects gathered further evidence of the presence of dark matter. Furthermore, the dark matter could explain the observations of the angular spectrum of the *cosmic microwave background*, the faint electromagnetic radiation filling all space with tiny anisotropies, that was accidentally discovered in 1965 by Arno Penzias and Robert Wilson [8].
Another astronomical observation which may suggest the presence of dark matter is the rotation curve of galaxies. In a spiral galaxy most of the mass is stored in a *bulge* region at the center, hence the gravitational potential can be approximated to that of an extended, spherical mass M of radius R and density ρ:

$$\phi(r) = \begin{cases} \frac{4}{3}\pi G\rho r^2 & \text{for} \quad r < R; \\ \frac{GM}{r} & \text{for} \quad r \geq R. \end{cases} \tag{1.4}$$

Reminding the virial theorem, $2K + U = 0$ where K and U are the mean kinetic and potential energy respectively, the mean velocity is: $< v >= \sqrt{\phi(r)}$. Therefore, the plot of the velocity with respect to the distance from the center of the bulge is expected to grow linearly for $r < R$ and to decrease as the inverse of the distance for $r \geq R$. In 1970 the astronomers Vera Rubin and Kent Ford [9] studied the rotation velocity of the Andromeda (M31) spiral galaxy and found that it is almost constant for $r \geq R$, so they hypothesized that the galaxy was surrounded by a dark matter halo contributing to the gravitational potential. After this observation, many other galaxies were studied and each showed the same rotation curve trend.
From these astronomical observations it has become clear that the luminous matter described by the Standard Model cannot account for the total density of the universe and that it is necessary to include the much grater contribution of invisible dark matter, formed by very weakly interacting particles. Dark matter is supposed to make up about 26% of the universe (compared to 68% of dark energy and 6% of ordinary matter) and it is expected to be cold (slowly moving with respect to the speed of light).

As QCD axion and ALPs could constitute dark matter, in the last forty years they have drawn the attention of many particle physicists and several experiments were proposed and carried out to search for these new particles. Since there was no new particle discovered with mass $\simeq 100\, keV$ (corresponding to the electroweak scale $f_{ew} \simeq 250\, GeV$), the interest was focused on *invisible axions*, e.g. the Dine-Fischler-Srednicki-Zhitnitskii (DFSZ) ([10], [11]) and the Kim-Shifman-Vainstein-Zakharov(KSVZ) ([12], [13]) model classes for QCD axions. Other ALPs models were theorized in String theory, Supergravity, Supersymmetry and Grand Unified Theory.
The invisible axion is much lighter and couples very weakly with SM particles ($m_a < eV$, $f_a >> f_{ew}$). Being bosons, many axions can occupy the same state. Thus, to account for local density of dark matter at the Milky Way Galactic halo $\rho_{DM} \simeq 0.3 \div 0.4\, GeV\ cm^{-3}$, the axion occupation number should be very high [6]:

$$n_a \simeq 3 \times 10^{14} \left(\frac{10^{-6}\, eV}{m_a}\right)\ \text{axions} \cdot \text{cm}^{-3} \tag{1.5}$$

resulting in a macroscopic wave-like behaviour that can be described using classical field theory:

$$a(t,\overline{x}) = \int d^3k\; e^{i\{\omega(\overline{k})t+\overline{k}\overline{x}\}}\; a(\overline{k}) \tag{1.6}$$

$$\langle a(\overline{k})\rangle = 0; \qquad \langle a(\overline{k})a(\overline{k'})^*\rangle = f_{MB}(|\overline{k}|)\delta^3(\overline{k}-\overline{k'}), \tag{1.7}$$

where $a(\overline{k})$ is the field mode of wave vector $\overline{k}$.
A dark matter axion field would have a local Maxwell-Boltzmann $f_{MB}(|\overline{k}|)$ velocity distribution with dispersion $\sigma_v \simeq 270$ km/s in the galactic frame of reference. Thus, from the axion dispersion relations:

$$E = \hbar\omega = m_a c^2 + m_a v_a^2/2; \qquad \overline{p} = \hbar\overline{k} = m_a\overline{v_a} \tag{1.8}$$

it is possible to estimate the frequency dispersion of the galactic halo axion field in the galactic frame:

$$\frac{\Delta\omega_a}{\omega_a} \simeq 5\times 10^{-7} \tag{1.9}$$

hence a dark matter axion signal would be extremely narrow. For an experiment on Earth, due to its orbital motion around the Sun and the rotational motion of the detector about its axis, the value in equation (1.9) is doubled so that the quality factor is $Q_{a,E} = (\Delta\omega_a/\omega_a)_E^{-1} \simeq 10^6$ [14].

The main issue about searching for the QCD axion is the determination of its mass $m_a \propto 1/f_a$: since it cannot be predicted by the theory, experiments need to scan a wide energy range depending on the source of the axion searched and on its interactions with ordinary matter. The QCD axion's interactions with SM fields and particles could be of three types: i) with the electromagnetic field ($g_{a\gamma\gamma}$), resulting in a feeble electric signal when an axion in a strong magnetic field is converted into a photon with frequency $\nu_a = m_a c^2/h$; ii) with fermion spins (g_{aff}); iii) with nuclear electric dipole moments (g_{EDM}). These three interactions are proportional respectively to [4]:

$$g_{a\gamma\gamma}\, a\mathbf{E}\cdot\mathbf{B};\;\; g_{aff}\,\nabla a\cdot\hat{\mathbf{S}};\;\; g_{EDM}\, a\hat{\mathbf{S}}\cdot\mathbf{E}, \tag{1.10}$$

where $\mathbf{E}$ and $\mathbf{B}$ are the electric and magnetic field respectively, $\hat{\mathbf{S}}$ is the spin vector of the particle interacting with the QCD axion. Experimental searches mainly focus on detecting the interaction with the EM field: an oscillating axion field *a(x,t)* would modify Maxwell's equations as [15]:

$$\nabla\cdot\mathbf{E} = \rho - g_{a\gamma\gamma}\,\nabla a\cdot\mathbf{B}; \quad \nabla\times\mathbf{B} - \dot{\mathbf{E}} = j + g_{a\gamma\gamma}(\dot{a}\mathbf{B} + \nabla a\times\mathbf{E}). \tag{1.11}$$

Since the de Broglie wavelength of the QCD axion field would be large for a mass range $\simeq 1\,\mu eV$, ∇a is approximately zero, thus only the time-dependent current density term $g_{a\gamma\gamma}\,\dot{a}\mathbf{B}$ can be detected in experiments.

The first detection principle to be proposed in 1983 by Pierre Sikivie [16] aimed at looking for axions that may have been converted to photons in a strong magnetic field. Since then, many experimental techniques have been developed to search for axions at different mass ranges [15].
Dark matter axions are expected to have masses in the μeV range and they may originate photons in the microwave frequency region. The signals from our galactic halo are looked for with the *haloscope* technique, which uses different kinds of resonators.
A first type of haloscope employs a microwave resonant cavity immersed in a strong magnetic field. If the frequency of an axion-induced photon is close to the resonant frequency of the cavity, its signal emerges as a tiny excess in the variance of the electric field in the cavity. Since the mass of the axion cannot be known a priori, cavities are built so that their resonant frequency can be tuned and at each tuning step the noise is mediated for a time sufficient to detect a potential excess in the variance of power fluctuations. Therefore haloscopes need much time to scan wide frequency ranges, depending on the detector's scan rate, which in turn is determined by the visibility (the ratio of the expected signal power spectral density to the total noise power spectral density) and by the visibility bandwidth (the characteristic bandwidth over which the haloscope is sensitive).
The first experiments with microwave cavities were carried out in 1987 by the Rochester-Brookhaven-Fermilab Collaboration. The sensitivity was too limited by the high system noise temperature (about

16K) to reach the predictions of KSVZ and DFSZ models of QCD axion. An experiment at the University of Florida improved the sensibility bringing the system noise temperature to 3K.
The ADMX (*Axion Dark Matter eXperiment*) was established in 1990 and was the first large-scale experiment sensitive to low-mass QCD axion regions ($1-10\mu eV$). The experiment was later enhanced deploying the *SQUID* (*Superconductive Quantum Interference Device*) technology and a dilution refrigerator in order to operate at sub-kelvin temperatures and to reduce the noise almost to the quantum limit. However, the searching for low-frequency axions (below 1 GHz) was limited by the large dimension of the cavity.
The HAYSTAC experiment (*Haloscope at Yale Sensitive to Axion Cold dark matter*) aimes at detecting dark matter axions with masses above 20 μeV. It is the first haloscope experiment with a high-quality-factor microwave resonant cavity ($Q \simeq 47000$, volume V=1.5 l, at temperature T=61mK) to squeeze the vacuum states through a pair of *Josephson Parametric Amplifiers* (*JPAs*) to reduce the noise beyond the fundamental quantum limit, increasing the scan rate of the detector and consequently its sensitivity bandwidth [1].

For high-frequency axions, dielectric haloscopes are used: periodic structures of dielectric walls with constant ϵ_r serve as open resonators, where it is possible to reach the 10-100 GHz frequency range (40-400 μeV mass region). This strategy was proposed by the MADMAX Collaboration (*Magnetized Disc and Mirror Axion eXperiment*) at DESY.

The aim of QUAX (*QUest for AXions*) haloscopes at INFN-LNL is to detect dark matter axions through their couplings to photons (QUAX-aγ) and electrons (QUAX-ae). QUAX-aγ uses a resonant cavity immersed in a strong magnetic field to detect DM axions converted into radio-frequency photons ($m_a = 30-50\ \mu eV$). QUAX-ae would be sensitive to the photons produced by the magnetic transitions excited by the effective rf magnetic field on electron spin in a magnetized sample, due to the motion of the solar system in the galaxy ($m_a \simeq 30 - 80\ \mu eV$).

Another possible source of axions are stars, from which the new particles would emerge after the conversion of photons in the stellar plasma via Primakoff effect, in the X-rays region (the total axion energy would reflect the Sun's interior temperature of a few keV, no matter what its mass is). These axions could be searched for through *helioscopes*, detectors sensitive to high-mass regions which use dipole magnets directed towards the Sun to look for X-rays signal excesses due to the axion-photon conversion in the magnetic field. Helioscopes experiments were held at the Brookhaven National Laboratories, then at the Tokyo University and lastly at the *CERN Axion Solar Telescope* (CAST) setting the most restrictive limit $1/f_a < 10^{-10} GeV^{-1}$ for $m_a < 0.02$ eV, resulting competitive with astrophysical limits. An enhanced helioscope, IAXO (*International Axion Experiment*), aims at improving CAST's sensibility.

Finally, if existing, the QCD axion and ALPs may be produced in the laboratory with the *Light Shining through a Wall* (*LSW*) technique: a strong light source emits photons which are converted into axions in a strong superconductive dipole magnet; these, being very weakly interacting particles, propagates through a wall opaque for photons and are again converted into photons with the same energy as the original by a similar magnet apparatus placed beyond the wall.
LSW experiments were first carried out by the Brookhaven-Fermilab-Rochester-Trieste Collaboration. The most stringent laboratory limit ($m_a < 0.3$ meV) was achieved by the OSQAR experiment (*Optical Search for QED vacuum bifringence, axions and photon Regeneration*) which deployed the LHC dipole magnets at CERN. A similar result was obtained by the *ALPS Collaboration* at DESY.

Chapter 2

Amplification of MW signals

Haloscopes provide the most sensitive technique to look for axion signals in the microwave range: the axion-photon conversion is enhanced in a tunable, high-Q microwave cavity immersed in a strong magnetic field at the resonant condition $h\nu = m_a c^2$. The expected axion signal power [15]:

$$P_a = 5.0 \times 10^{-23}\ W \left(\frac{g_\gamma}{0.75}\right)^2 \left(\frac{\rho_a}{0.45\ GeV\ cm^{-3}}\right) \left(\frac{\nu_a}{1\ GHz}\right) \left(\frac{B_0}{10\ T}\right)^2 \left(\frac{V}{30\ L}\right) \left(\frac{G}{0.5}\right) \left(\frac{Q}{10^5}\right) \quad (2.1)$$

is proportional to the coupling parameter g_γ (1.92 and 0.75 for the KSVZ and DFSZ models respectively), the DM local mass density ρ_a, the Compton frequency of the axion ν_a, the applied external magnetic field B_0, the volume V of the cavity and its geometrical factor G and quality factor Q.
Since the frequency ν_a is not known a priori, the cavity is tuned in small steps and at each one the signal is acquired for a sufficient time to detect, if present, an excess of power over the noise due to the axion. The signal-to-noise ratio is given by the Dicke radiometer equation [17]:

$$\frac{S}{N} = \frac{P_a}{k_B T_N} \cdot \sqrt{\frac{\tau}{\Delta\nu_s}}, \quad (2.2)$$

in which T_N is the noise temperature (see equation (2.3)), τ is the integration time at each step and $\Delta\nu_s$ is the frequency bandwidth of the axion signal (see equation (2.33)). This equation points out the main shortcomings of the haloscope technique: first of all, since the axion signal is expected to be narrow-band and very feeble ($P_a \simeq 10^{-23}$ W), very tiny tuning steps are needed and each step requires a long integration time in order to maximize the signal-to-noise ratio; furthermore, even in the lowest-noise linear amplifiers the so-called *standard quantum limit* (SQL) prevails over other noise sources and cannot be overcome classically.
To the SQL is associated a temperature such that, at each frequency, $k_B T_{SQL} = \hbar\omega$. It emerges at zero temperature from the expression of the total system noise temperature T_N, which is the sum of two terms:

$$k_B\, T_N = \hbar\omega \left(\frac{1}{e^{\hbar\omega/k_B T} - 1} + \frac{1}{2}\right) + k_B\, T_A\ . \quad (2.3)$$

The first term accounts for the fluctuations in the cavity at a given temperature T (see equation (2.18)). At zero temperature, it contributes to half of the SQL, the other half arising from the minimum noise energy provided by a linear amplifier, i.e. $k_B T_{A,min} = \hbar\omega/2$ (see equation (2.30)).
The first haloscope experiments tried to reduce T_N by lowering the system temperature T: amplifiers with $T_N = 5 \div 20$ K were used at the Rochester-Brookhaven-Fermilab Collaboration and at the University of Florida, approximately 200 times the T_{SQL} over the range $\nu \simeq 1 - 3$ GHz. The ADMX experiment in the mid 1990s used amplifiers based on *High-Electron-Mobility Transistors* (*HEMT*) improving the noise temperature to $\simeq 200\ T_{SQL}$ at $\nu <$ GHz. In 1998 Clarke and collaborators invented an amplifier based on *microstrip-coupled SQUID amplifier* (*MSA*) at ADMX and were able to bring the system's T_N to about 15 T_{SQL}. It was the HAYSTAC experiment to first employ the JPAs to lower the temperature noise to around 2 T_{SQL} with a cavity smaller than the one at ADMX.

2.1 Stochastic processes

The single execution of physics experiments can be regarded as a statistical ensemble: due to the sources of random noise, the output at a fixed time can be described as a random variable. After the execution, each possible outcome evolves in a deterministic way and therefore it is a function of time *u(t)*. Thanks to the ergodicity of the system [18], its time average tends to the ensemble average value (2.4). The set of all the functions *u(t)* whose values at a given time t is a random variable is called *stochastic process*.
For stochastic processes with statistical properties given by the probability distribution function *f(u,t)* it is possible to define the *average value*, the *auto-correlation function* and the *auto-covariance*:

$$\eta(t) = E[u(t)] = \int_{-\infty}^{\infty} u\, f(u,t)\, du; \tag{2.4}$$

$$R(t,t') = E[u(t)u(t')] = \int_{-\infty}^{\infty}\int_{-\infty}^{\infty} u\, u' f(u,u',t,t')\, du\, du'; \tag{2.5}$$

$$C(t_1,t_2) = R(t_1,t_2) - \eta(t_1)\eta(t_2). \tag{2.6}$$

It is worth noticing that $R(t,t) = E[u^2(t)]$ and that $C(t,t)$ is the variance of the random variable $u(t)$. A stochastic process is said to be *stationary* if it is invariant under time translations: $u(t+t') = u(t)$. It follows that the auto-correlation function of a stationary process only depends on time intervals, $R(t,t') = R(t-t') \equiv R(\tau)$. The *power spectrum* for stationary processes is defined as the Fourier transform [1] of $R(\tau)$:

$$S(\omega) = \int_{-\infty}^{\infty} R(\tau)\, e^{-i\omega\tau}\, d\tau. \tag{2.7}$$

In particular, at $\tau = 0$ the integral of the power spectrum is proportional to the mean power of the process:

$$R(0) = E[u^2] = \frac{1}{2\pi}\int_{-\infty}^{\infty} S(\omega)\, d\omega. \tag{2.8}$$

During an experiment, incoming signals are stochastic processes $i(t)$ which are transformed by the detection chain $T[\cdot]$ into other stochastic processes with the same statistical properties: $u(t) = T[i(t)]$. If the fluctuations of the incoming signals are small, it is possible to linearize the system:

$$u(t) = \int_{-\infty}^{\infty} h(t,\tau)\; i(\tau)\; d\tau, \tag{2.9}$$

where $h(t,\tau)$ is a function of time.
In a linear system, if the input is stationary and also the transfer function is stationary, so that $h(t,t') = h(t-t')$, then the output is stationary as well and the simple expressions below follow:

$$E[u] = E[i]\int_{-\infty}^{\infty} h(\tau)\, d\tau; \tag{2.10}$$

$$R_{uu}(\tau) = \int_{-\infty}^{\infty}\int_{-\infty}^{\infty} h(\tau')\, h(\tau'')\, R_{ii}(\tau - \tau' + \tau'')\, d\tau'\, d\tau''. \tag{2.11}$$

Therefore, it is possible to easily find the useful relation:

$$S_u(\omega) = |h(\omega)|^2 S_i(\omega), \tag{2.12}$$

where $h(\omega)$ in the Fourier transform of the transfer function $h(t)$.

[1] Here and in the following, $g(t) = (1/2\pi)\int_{-\infty}^{\infty} \hat{g}(\omega)e^{i\omega t}d\omega$ and $\hat{g}(\omega) = \int_{-\infty}^{\infty} g(t)e^{-i\omega t}dt$

2.2 Johnson–Nyquist noise

An intrinsic source of noise in real electric systems is the thermal noise due to the ohmic dissipation arising from the scattering of the charge carriers from the other degrees of freedom of the system. It is possible to describe this phenomenon by adding to the mean current I_0 through a resistor a white noise current I_n: a stochastic normal process with zero mean value and auto-correlation $R_{I_nI_n}(\tau) = P\delta(\tau)$ where P =const. If the system is short-circuited by an inductor (figure 2.1 (c)), the power spectrum of the noise current is $S_{II}(\omega) = P/(1+\omega^2\hat{\tau}^2)$ with $\hat{\tau} = L/R$. Then, from the equipartition theorem, $E[I^2]L/2 = k_BT/2$ and $E[I^2] = 1/(2\pi)\int S_{II}(\omega)d\omega = P/2\hat{\tau}$ hence $P = 2k_BT/R$. Therefore the thermal noise can be modelled as an ideal resistor with a stochastic normal, zero mean value current generator in parallel or equivalently with a voltage generator in series, with power spectrum given by the *Nyquist relation* (figure 2.1 (a-b)) [18]:

$$S_{I_nI_n}(\omega) = 2k_BT/R \text{ or } S_{V_nV_n}(\omega) = 2k_BTR. \tag{2.13}$$

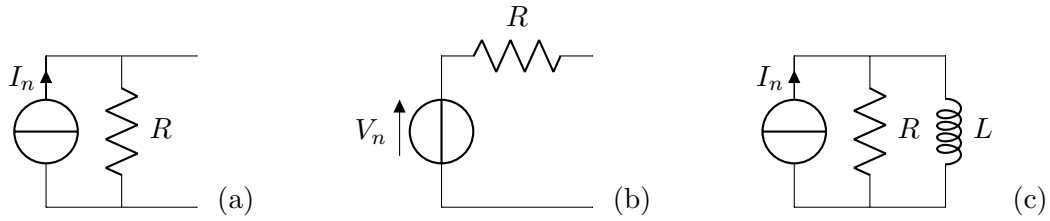

Figure 2.1: a-b)Equivalent models of a real resistor; c)resistor and inductor in parallel.

In general, a port of impedance $Z(\omega)$ short-circuited by a resistor dissipates a mean power

$$P_R = E\left[\int_{-\infty}^{\infty} I(t)V(t)dt\right] = \int_{-\infty}^{\infty} R_{IV}(\tau)d\tau, \tag{2.14}$$

where $I(t)$ and $V(t)$ are the current and voltage through the port. In the frequency domain, $I_n(\omega) = V_n(\omega)/[Z(\omega)+R]$ where $V_n(\omega)$ is the voltage of the noise generator. Using Parseval's theorem,

$$P_R = \frac{1}{2\pi}\int_{-\infty}^{\infty}\frac{Z(\omega)2k_BTR}{|Z(\omega)+R|^2}d\omega = \frac{1}{2\pi}\int_{-\infty}^{\infty}\frac{Re\{Z(\omega)\}2k_BTR}{|Z(\omega)+R|^2}d\omega, \tag{2.15}$$

where the imaginary part is an odd function and does not contribute to the integral (since the impedance is real quantity, $Z(\omega) = Z^*(-\omega)$). If a noise generator of power spectrum $S_Z(\omega)$ is associated to the impedance $Z(\omega)$ then the power dissipated in R is:

$$P_Z = \frac{1}{2\pi}\int_{-\infty}^{\infty}\frac{S_Z(\omega)R}{|Z(\omega)+R|^2}d\omega \tag{2.16}$$

and since at equilibrium $P_R = P_Z$, it follows that

$$S_Z(\omega) = 2k_BTRe\{Z(\omega)\}. \tag{2.17}$$

In an article published in 1951 [19] H.B. Callen and T.A. Welton used the formalism of quantum perturbation theory to extended the Nyquist relation, founding that the power spectrum arising from the thermal excitation at temperature T of electrons in an oscillating system of frequency ω has the correct expression:

$$S_Z = 2\hbar\omega\coth\left(\frac{\hbar\omega}{2k_BT}\right)Re(Z(\omega)) \tag{2.18}$$

so that, at the standard quantum limit, this source of noise contributes to the total noise energy as half of the irreducible single quantum of noise.

2.3 Noise in linear amplifiers

A linear amplifier multiplies a very feeble input signal by a high-modulus linear transfer function. As a consequence, the output signal is usually great enough to make the noise sources after the amplifier negligible, in particular the perturbations predicted by the Heisenberg principle can be ignored. It follows that the output signal can be measured classically and it carries information about the input signal that is to be described quantum mechanically. Therefore, a real linear amplifier must be associated to voltage ($S_{V_nV_n}$) and current ($S_{I_nI_n}$) noise generators that disturb the physical quantity complementary to the one being measured in order to restore the uncertainty principle. As a consequence, it is possible to define an amplifier's noise temperature $k_BT_A = \sqrt{S_{V_nV_n}S_{I_nI_n}}$ and a noise resistance $R_n = \sqrt{S_{V_nV_n}/S_{I_nI_n}}$.
Around its resonance frequency ω_0, the microwave cavity behaves like a RLC circuit with characteristic impedance:

$$Z(\omega) = \frac{i\omega}{C}\frac{1}{\omega_0^2 - \omega^2 + i\omega\omega_0/Q}, \tag{2.19}$$

where $Q = \omega_0 RC = R/(\omega_0 L)$ is the quality factor. The equivalent circuit of the cavity and the amplifier around ω_0 is shown in figure 2.2, where the Johnson-Nyquist noise associated to the resistor R has been included in the amplifier's noise current generator $S_{I_nI_n}$.

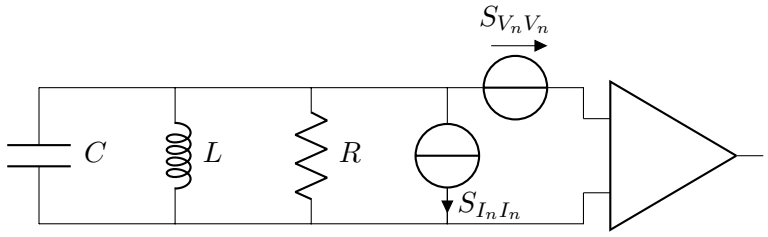

Figure 2.2: Equivalent circuit of a cavity and an amplifier.

The noise voltage at the amplifier's input is a zero mean value, normal stochastic process with power spectrum:

$$S_{VV} = S_{V_nV_n} + |Z(\omega)|^2 S_{I_nI_n} + \alpha ReZ(\omega), \tag{2.20}$$

where $\alpha = 2k_BT$ at high temperatures and $\alpha = 2\hbar\omega \coth \frac{\hbar\omega}{k_BT}$ at low ones (see equations (2.17) and (2.18)). At the resonance frequency $\omega = \omega_0$, the minimum of S_{VV} is found for $R_n = Q/(C\omega_0)$, so that:

$$S_{VV} = \frac{\omega_0\omega^2}{QC}\frac{1}{(\omega_0^2 - \omega^2)^2 + \omega^2\omega_0^2/Q^2}\, 2k_BT_{eq} \tag{2.21}$$

hence the presence of the amplifier increases the equivalent temperature of the system $T_{eq} = \alpha/(2k_B) + T_A$. The variance of the voltage is:

$$\sigma_V^2 = \frac{1}{2\pi}\int S_{VV}(\omega)d\omega = \frac{1}{2\pi}2k_BT_{eq}\frac{\omega_0}{QC}\int \frac{\omega^2}{(\omega_0^2 - \omega^2)^2 + \omega_0^2\omega^2/Q^2}d\omega = \frac{k_BT_{eq}}{C}. \tag{2.22}$$

Since the process has zero mean value, σ_V^2 is proportional to the mean value of the noise energy $\langle E_n\rangle = C\langle V^2\rangle/2 = C\sigma_V^2/2$ and equation (2.22) is in agreement with the equipartition theorem for $T = T_{eq}$: $C\sigma_V^2 = k_BT_{eq}$.
Neglecting the generators and the resistor, the system including the charge Q on the capacitor and the flux φ through the inductor is described by the Hamiltonian:

$$H = \frac{Q^2}{2C} + \frac{\varphi^2}{2L} \tag{2.23}$$

which is the Hamiltonian of the harmonic oscillator with Q and φ replacing the position and momentum (in the real circuit, the resistor would couple this oscillator to the whole system) and, according to the Heisenberg principle, in a state of minimum uncertainty $\sigma_Q\sigma_\varphi = \hbar/2$.

Let suppose that the oscillator has initial condition $\varphi = 0$ at $t = 0$. At $t > 0$ a measure of the voltage at the output of the linear amplifier begins and the output signal is mediated over a time interval $T << 1/\omega_0 << \tau$, where $\omega_0 = (LC)^{-1/2}$ is the natural frequency of the oscillator and $\tau = RC$ is the damping parameter. This is equivalent to a measure of the charge:

$$Q = \frac{1}{T}\int_0^T CV(t)dt \tag{2.24}$$

so that the charge is itself a stochastic process of variance:

$$\sigma_Q^2 = \frac{1}{T^2}\int_0^T\int_0^T C_Q(t-t')dtdt' = \frac{1}{T}\int_{-T}^T C_Q(\tau)\left(1-\frac{|\tau|}{T}\right)d\tau, \tag{2.25}$$

where $C_Q(\tau)$ is the auto-covariance of the process $Q(t) = CV(t)$ and V is the voltage at the input of the amplifier. If the voltage process is white until $\omega >> 1/T$, so that $S_V(\omega_0) = S_V$ and $R_V(t) = S_V\delta(t)$, and if it has zero mean value then also the charge process has zero mean value and auto-covariance function $C_Q(t) = C^2 S_V\delta(t)$, so that:

$$\sigma_Q^2 = C^2 S_V/T. \tag{2.26}$$

The magnetic flux power spectrum is $S_\varphi(\omega) = S_I|Z(\omega)|^2/\omega^2$ and, assuming that $S_I(\omega) = S_I(\omega_0) = S_I$, its auto-correlation is:

$$R_\varphi = (S_I\tau/2\omega_0^2C^2)e^{-t/2\tau}[\cos(\omega_1 t) - (1/2\omega_1\tau)\sin(\omega_1\tau)]), \tag{2.27}$$

where $\omega_1^2 = \omega_0^2 - 1/4\tau^2 \simeq \omega_0^2$. Finally, expanding to the first order in $1/2\tau$:

$$\sigma_\varphi = E\{[\varphi(T) - \varphi(0)]^2\} = 2R_\varphi(0) - 2R_\varphi(T) = S_I\tau/C^2\omega_0^2. \tag{2.28}$$

In conclusion:

$$\sigma_\varphi\sigma_Q = (S_I S_V)^{1/2}/\omega_0 = W(\omega_0)/\omega_0 = \hbar/2 \tag{2.29}$$

hence the minimum noise energy from a linear amplifier is equal to the zero-point energy of the harmonic oscillator:

$$W(\omega_0) = \frac{1}{2}\hbar\omega_0 \equiv k_B T_{A,min}. \tag{2.30}$$

2.4 Radiometer equation

With reference to figure 2.2, if an external voltage signal is present, it contributes to the power spectrum as $S_{VV}(\omega) = |Z(\omega)|^2 S_s(\omega)$. When the signal bandwidth is $\Delta\omega_s << \Delta\omega_{RLC} = \omega_0/Q$, as it is expected from an axion signal, the variance can be approximated as:

$$\sigma_s^2 = \frac{1}{2\pi}\int |Z(\omega)|^2 S_s(\omega)d\omega \simeq \frac{1}{2\pi}\Delta\omega_s S_{VV}(\omega = \omega_0). \tag{2.31}$$

Therefore, the signal increases the noise mean value up to $k_B T_{eq}/C + \sigma_s^2/C$.
In order to detect the signal, the fluctuation $\sigma_{V^2} = \sqrt{2}\sigma_V^2$ [18] of the noise around the mean value should be smaller. If a sample of N measures of V^2 is acquired in a time interval τ, the mean value has variance $\sigma_V^2/\sqrt{N}$ provided that the measures are statistically-independent, therefore τ must be greater or equal to the correlation time of the signal. From the Nyquist sampling theorem, a sampling interval of τ/N corresponds to a bandwidth $\Delta\nu = N/(2\tau)$, so that $N = 2\Delta\nu\tau$ and $\tau \simeq 1/\Delta\nu$. Therefore, the measures can be considered statistically independent if $\tau \geq 1/\Delta\nu_s$ and consequently $N = 2\Delta\nu_s\tau$ and the variance of the mean value of the noise is:

$$\sigma_N^2 = \sqrt{2}\frac{\sigma_V^2}{\sqrt{N}} = \frac{\sigma_V^2}{\sqrt{\Delta\nu_s\tau}}. \tag{2.32}$$

The Dicke radiometer equation follows straightforward:

$$\frac{S}{N} = \frac{\sigma_s^2}{\sigma_N^2} \simeq \frac{P_a/\Delta\nu_s}{\sigma_V^2/(\sqrt{\Delta\nu_s\tau})} = \frac{P_a}{k_B T_N}\sqrt{\frac{\tau}{\Delta\nu_s}}. \tag{2.33}$$

Chapter 3

Microwave squeezing

3.1 Squeezed states of electromagnetic radiation

The general solution of the classical wave equation for an electromagnetic field propagating in vacuum,

$$\nabla^2 \mathbf{E}(\mathbf{r},t) - \frac{1}{c^2}\frac{\partial^2}{\partial t^2}\mathbf{E}(\mathbf{r},t) = 0 \tag{3.1}$$

is the electric field vector of complex amplitude $\alpha(\mathbf{r},t) = \alpha_0(\mathbf{r},t)e^{i\phi(\mathbf{r},t)}$ (α_0 being the real amplitude and ϕ the total phase), oscillating at frequency $\nu = \omega/2\pi$ with polarization $\mathbf{p}(\mathbf{r},t)$:

$$\mathbf{E}(\mathbf{r},t) = E_0[\alpha(\mathbf{r},t)e^{i\omega t} + \alpha^*(\mathbf{r},t)e^{-i\omega t}]\,\mathbf{p}(\mathbf{r},t). \tag{3.2}$$

Such solution can be expressed equivalently in terms of the so-called *amplitude quadrature* $X_1 = \alpha^*(\mathbf{r},t) + \alpha(\mathbf{r},t)$ and *phase quadrature* $X_2 = i[\alpha(\mathbf{r},t) - \alpha^*(\mathbf{r},t)]$ as:

$$\mathbf{E}(\mathbf{r},t) = E_0[X_1\cos(\omega t) + X_2\sin(\omega t)]\,\mathbf{p}(\mathbf{r},t). \tag{3.3}$$

The classical energy of the electromagnetic wave passing through the infinitesimal surface $dx \cdot dy$ around the point (x,y) in the time interval dt around t is

$$\epsilon(x,y,t) = E_0^2\, 2\alpha\alpha^*\, dt\, dx\, dy \qquad \text{or} \qquad \epsilon(x,y,t) = E_0^2\,(X_1^2 + X_2^2)\, dt\, dx\, dy, \tag{3.4}$$

where $E_0^2 = \hbar\omega/4$ [20]. Consequently, the classical Hamiltonian for a radiation made up of different frequency modes ω_k is:

$$H = \Sigma_k \frac{\hbar\omega_k}{4}(X_1^2 + X_2^2) \tag{3.5}$$

which is the Hamiltonian of multiple independent harmonic oscillators with canonical variables $q_k = \sqrt{\hbar\omega_k/2}\,X_{1,k}$ and $p_k = -\sqrt{\hbar/(2\omega_k)}\,X_{2,k}$.

It is possible to apply the canonical quantization to the Hamiltonian (3.5) by introducing the operators $\hat{q}_k$ and $\hat{p}_k$ which satisfy the commutation rule $[\hat{q}_k, \hat{p}_l] = i\hbar\delta_{kl}$. In the quantum description of electromagnetic waves, the complex amplitude α_k is replaced by the operator $\hat{a}_k$ defined in frequency space. This operator together with its adjoint $\hat{a}_k^\dagger$ raise and lower respectively the excitation of a mode by one photon and they satisfy the Boson commutation rules: $[\hat{a}_\nu, \hat{a}_{\nu'}^\dagger] = \delta_{\nu,\nu'}$ and $[\hat{a}_\nu, \hat{a}_{\nu'}] = [\hat{a}_\nu^\dagger, \hat{a}_{\nu'}^\dagger] = 0$. By analogy with the classical description, $\hat{X_1} = \hat{a} + \hat{a}^\dagger$ and $\hat{X_2} = i(\hat{a}^\dagger - \hat{a})$ so that in the representation of the quadrature operators:

$$\hat{H} = \Sigma_k \frac{\hbar\omega}{4}(\hat{X}_{1,k}^2 + \hat{X}_{2,k}^2); \qquad [\hat{X}_{1,k}, \hat{X}_{2,l}] = 2i\delta_{kl}, \tag{3.6}$$

where each quantum oscillator in the sum has energy $\epsilon_k = (n + 1/2)\hbar\omega_k$ in the eingenstate $|n>$ of the *number operator* $\hat{N} = \hat{a}^\dagger\hat{a}$ of eigenvalue n representing the number of photons of energy $\hbar\omega_k$ that

make up the field.
Because of the non-zero commutation relation in (3.6), the two quadrature operators do not have simultaneous eigenstates and from the uncertinty principle it follows that:

$$<\Delta\hat{X}_1^2><\Delta\hat{X}_2^2> \geq 1 \tag{3.7}$$

The *coherent states* $|\alpha>$ are minimum uncertainty states defined as the eigenstates of the lowering operator, $\hat{a}|\alpha> = \alpha|\alpha>$, such that the intensity of the state is $\alpha\alpha^* = |\alpha|^2$. They can be obtained from the vacuum state as: $|\alpha> = \hat{D}(\alpha)|0>$ in which $\hat{D}(\alpha) = \exp(\alpha\hat{a}^\dagger - \alpha^*\hat{a})$ is the unitary displacement operator. For these states, the uncertainty is equally split between the two quadratures:

$$<\Delta\hat{X}_1^2>_\alpha = <\Delta\hat{X}_2^2>_\alpha = 1 \tag{3.8}$$

Every state of an electromagnetic wave can be represented in a so-called *phasor diagram* of the quadrature operators, that is a plot of $\hat{X}_2$ versus $\hat{X}_1$ (see figure 3.1, [21]). Each coherent state is equivalent to a circular area of radius $<\Delta\hat{X}_1^2> = 1$ centered around the value of coordinates $(<\hat{X}_1>, <\hat{X}_2>)$ which describes the extent of the uncertainty distribution. In particular, the uncertainty area is symmetric and independent on the intensity $|\alpha|^2$ of the state. Such uncertainty does not depend on the technical imperfections of the instrumental apparatus, but rather it emerges as an intrinsic source of quantum noise.

It is possible to generate minimum uncertainty states affected by less noise in one quadrature than in the standard quantum limit. As a consequence the noise in the orthogonal quadrature increases in order to restore the Heisenberg principle and the distribution function is no longer symmetric. These states are called *squeezed states of light* and in the phasor diagram are represented by an ellipse with the semi-minor axis aligned to the squeezing direction (figure 3.1 (c)).
Squeezed states are represented by kets in the form $|\alpha, \xi>$ with $\xi = r_s e^{i2\theta_s}$ where α^2 is the intensity of the state, θ_s and r_s are the orientation and degree of squeezing respectively. Given a generic quadrature $\hat{X}(\theta) = e^{-i\theta}\hat{a} + e^{i\theta}\hat{a}^\dagger$, the variance in a squeezed state is:

$$Var(\hat{X}(\theta)) = \cosh(2r_s) - \sinh(2r_s)\cos(2(\theta - \theta_s)) \tag{3.9}$$

and it has a minimum when $\theta = -\theta_s$ and a maximum in the orthogonal direction $\theta = -\theta_s + \pi/2$. In the frame of reference rotated by the angle θ_s with regard to the quadrature amplitudes $\hat{X}_1, \hat{X}_2$, so that $\hat{Y}_1 + i\hat{Y}_2 = (\hat{X}_1 + i\hat{X}_2)e^{-i\theta_s}$, the variances take the simple expressions:

$$<\Delta\hat{Y}_1^2> = e^{-2r_s}; \qquad <\Delta\hat{Y}_2^2> = e^{2r_s} \tag{3.10}$$

thus the minor and major semi-axes of the ellipse in the phasor diagram are respectively of the size $\sigma_{X_1} = e^{r_s}$ and $\sigma_{X_2} = e^{-r_s}$. The squeezing is then defined as the ratio between the variances of the vacuum state $\sigma_{vac} = 1$ and the squeezed quadrature:

$$S = \sigma_{X_2}^2/\sigma_{vac}^2 = e^{-2r_s} \quad \text{or equivalently} \quad -10\log_{10}(S) = -10\log_{10}(e^{-2r_s}) \ [dB] \tag{3.11}$$

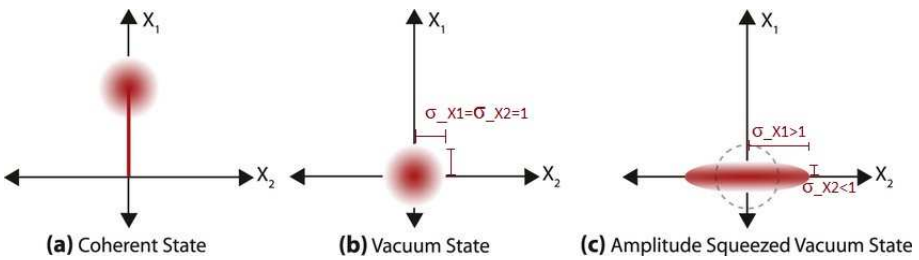

Figure 3.1: Quantum phasor diagram representations of various quantum light states [21].

3.2 Benefits from squeezing

In a haloscope experiment, the microwave cavity modes can be described as single quantum harmonic oscillators, the electric field being the oscillating quantity described by its slow varying cosine and sine components as in equation (3.3). The axion field is supposed to couple to one of this modes and alter its state in the (X_1, X_2) phase space, leading to a displacement which on average yields a small excess power above the quantum fluctuations, isotropic in quadrature space.
Even though the cavity is immersed in a dilution refrigerator and therefore continuously prepared in its ground state of minimum uncertainty, the zero-points fluctuations (equation (3.8)) preclude the localization of the state beyond the Heisenberg uncertainty and measurements of the two quadrature amplitudes generate noise sources such that the apparent average energy of the oscillator is at least the standard quantum limit value of $\hbar\omega$, as follows from equation (2.3).
The HAYSTAC experiment overcomes this standard quantum limit by coupling the cavity to a *Squeezed State Receiver (SSR)* comprising a pair of JPA's [22] (see equation (4.40)). The first JPA, the *Squeezer (SQ)*, squeezes the input Johnson-Nyquist fluctuations arising from a $50\,\Omega$ termination along one quadrature; as a consequence, the corresponding variance is reduced below the vacuum level and the variance of its conjugate observable is amplified, thus preserving the uncertainty principle:

$$\sigma^2_{X_1} > 1\,; \qquad \sigma^2_{X_2} < 1. \tag{3.12}$$

This squeezed input field enters the cavity and, if an axion field is present, it is displaced in the phasor diagram. Finally, the displaced output field reaches the second JPA called *Amplifier (AMP)* where only the X_2 quadrature is noiselessly amplified with sufficient gain to overwhelm the noise added by the following amplification and mixing.

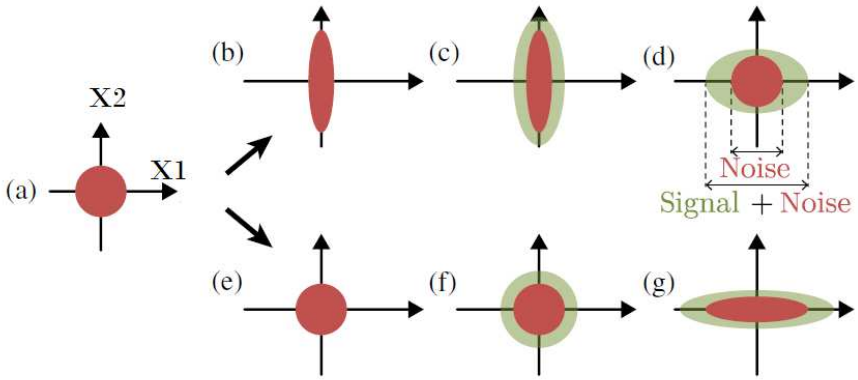

Figure 3.2: Phasor diagram of a coherent state (e-f-g) compared to a squeezed state (b-c-d) displaced by the axion field and amplified by the AMP [22].

In closing, the expression for the scan rate, i.e. the range of frequencies which the detector can scan during the time interval τ, follows from plugging equation (2.1) into equation (2.33) [15]:

$$R = \frac{d\nu}{d\tau} = \frac{12GHz}{yr}\left(\frac{5}{SNR}\right)^2\left(\frac{V}{30\,L}\right)^2\left(\frac{B_0}{10\,T}\right)^4\left(\frac{G}{0.5}\right)^2\left(\frac{g_\gamma}{0.75}\right)^4\left(\frac{\rho_a}{0.45\,GeV\,cm^{-3}}\right)^2 \cdot\left(\frac{20mK}{T_N}\right)^2\left(\frac{\nu_a}{1\,GHz}\right)^2\left(\frac{10^5}{Q}\right)^2. \tag{3.13}$$

By squeezing one quadrature of the vacuum, the noise fluctuations σ^2_N decrease by a factor S (see equation (5.4)) and, keeping S/N constant, from the radiometer equation (2.33) $\sqrt{\Delta\nu_s/\tau}$ increases by the same amount S, so that the scan rate R is improved. Finally, from a deliverable squeezing of 4 dB, R is roughly doubled [1].

Chapter 4

Josephson Parametric Amplifier (JPA)

4.1 Superconductivity

In 1911 Onnes was the first to observe in metals, which appear to lose their electrical resistance if held below a characteristic temperature T_c, the flow of a *supercurrent*, with a decay time experimentally estimated to be at least 10^6 years. However, superconductivity cannot be explained as a result of the infinite conductivity of a normal metal, since this model does not explain its magnetic properties. Among these, the *Meissner effect*: when a superconductor is cooled through T_c in a weak magnetic field (less than the critical field H_c, above which SC properties are destroyed), the magnetic flux is expelled from the SC metal, whereas Faraday's and Ohm's laws ($\nabla \times \mathbf{E} = -\partial \mathbf{B}/\partial t$; $\mathbf{j} = \sigma \mathbf{E}$) applied to a metal with conductivity $\sigma = \infty$ would predict that the flux is frozen in the bulk of the material. In particular, the Meissner effect requires that inside the superconductor $\mathbf{B} = \mu_0 \mathbf{H} + \mu_0 \chi \mathbf{H} = 0$, so that it achieves perfect diamagnetism ($\chi = -1$) and screens out completely the external applied field. Almost 50 years later (1957) Bardeen, Cooper and Schrieffer formulated a microscopic theory (BCS, [23]). Their hypothesis was that superconductivity in metals is represented by an ordered state of the conduction electrons: a first electron interacts with the lattice and deforms it so that a second one sees the deformation and takes advantage of it to lower its energy hence leading to an effective attraction between electron pairs, called Cooper pairs, via the lattice. Specifically, the BCS theory shows that in presence of an effective attraction the ground state of the metal is superconducting and separated by the closest excited state by a finite energy gap E_g.
Another theory that can account for the Meissner effect and other superconductivity features is the *Ginzburg-Landau (GL) theory*, which lays emphasis on the macroscopic quantum nature of this phenomenon [24]. In fact, it associates to the SC state a complex order parameter

$$\psi(r) = \psi_0 \, e^{i\phi(r)} \tag{4.1}$$

that can be considered as a macroscopic quantum wave function such that $|\psi(r)|^2 = n(r)$ is the fraction of SC electron, which is zero at T_c and unity at T=0 The GL theory addresses the temperature range near T_c where it is possible to expand the Gibbs free energy density f in a Taylor expansion in $|\psi|^2$ (or equivalently in *n(r)*):

$$f = f_0 + \alpha|\psi|^2 + (\beta/2)|\psi|^4 + (1/2m)|(-i\hbar\nabla - 2e\mathbf{A})\psi|^2, \tag{4.2}$$

where α and β are temperature-dependent and the last term in the expansion is the generalized kinetic energy quantum operator in the presence of an external magnetic field. Ginzburg and Landau demonstrated that near T_c, retaining the first order terms in $(T - T_c)$, the parameters could be written as $\alpha = \alpha_0(T - T_c)$ and β =const., consequently the minimum of f with respect to ψ satisfies a Schrödinger equation plus a nonlinear term:

$$(1/2m)(-i\hbar\nabla + 2e\mathbf{A})^2\psi + \alpha\psi + \beta|\psi|^2\psi = 0 \tag{4.3}$$

and it is possible to define a characteristic length over which the order parameter changes significantly: $\xi(T) = (\hbar^2/2m\alpha)^{1/2}$.
As known from quantum mechanics, the presence of an external magnetic field $\mathbf{B} = \nabla \times \mathbf{A}$ modifies the wave function of a single particle of mass m and charge q by adding the phase:

$$\delta\phi = \frac{q}{\hbar}\int \mathbf{A}\cdot d\mathbf{l}. \tag{4.4}$$

Since the order parameter can be considered as a wave function and it must be single-valued, the phase variation over a closed path must be an integer multiple of 2π and applying Stokes' theorem to the line integral leads to:

$$\delta\phi = \frac{2e}{\hbar}\int \nabla\times\mathbf{A}\cdot d\mathbf{S} = \frac{2e}{\hbar}\int \mathbf{B}\cdot d\mathbf{S} = \frac{2e}{\hbar}\Phi = 2n\pi, \tag{4.5}$$

where the current carriers are supposed to have charge 2e (as predicted by the BCS theory). The resulting flux is quantised:

$$\Phi = \frac{nh}{2e} = n\Phi_0. \tag{4.6}$$

If the bulk of superconductor is not simply connected, the sum of the flux generated by the supercurrent i_s flowing on the surfaces and the external applied flux is quantised:

$$\Phi = \Phi_{ext} + Li_s = n\Phi_0, \tag{4.7}$$

where $L = V_s(di_s/dt)^{-1}$ is the supercontuctor inductance.
Other SC effects important for electronics are the Josephson effects, which arise in the so called *Josephson junction*: when two pieces of superconductor in an external magnetic field (below the critical field H_c) are separated by a small region of weakened superconductivity, by quantum tunnelling the electrons in the first SC have non-zero probability to disrupt their pairing to other electrons and to cross the barrier, giving rise to a current density $\mathbf{j}$. As a result, in the junction there is an additional phase factor to the SC wave function:

$$\nabla\phi' = \frac{m\mathbf{j}}{2e\hbar|\psi|^2} + \frac{2e\mathbf{A}}{\hbar} \qquad \text{hence} \qquad \phi' = \frac{m\int_1^2 \mathbf{j}\cdot d\mathbf{l}}{e\hbar|\psi|^2}, \tag{4.8}$$

where the integral is over a path across the weak-link region in which the magnetic flux is negligible. Considering a SC ring interrupted by a Josephson junction, this phase contribution modifies the single-valued condition of the wave function:

$$\phi' + \frac{2e}{\hbar}\int_1^2 \mathbf{B}\cdot d\mathbf{S} = \phi' + 2\pi(\Phi_{ext} + Li_s)/\Phi_0 = 2n\pi, \tag{4.9}$$

where the integral is to be taken from one side of the junction to the other. Josephson showed that, in the limit of very weakly coupling, the supercurrent in the junction is periodic in Φ/Φ_0:

$$i_s = i_c \sin[2\pi(n - \Phi/\Phi_0)] = i_c \sin(\phi'), \tag{4.10}$$

where the critical current i_c is the maximum supercurrent which can flow through the junction.
The second Josephson effect emerges when a time-varying external flux is applied to a SC ring with Josephson junction. By the Faraday's law, if the flux is linearly varied a constant voltage drop appears across the junction: $V = -d\Phi_{ext}/dt$ =const. From the first Josephson relation,

$$i_s = i_c \sin[2\pi(Vt + Li_s)/\Phi_0] = i_c \sin(\phi) \tag{4.11}$$

hence a constant voltage generates a linear increase of the phase in time:

$$\frac{d\phi}{dt} = \frac{2eV}{\hbar} = \frac{\Phi_0}{2\pi}V, \tag{4.12}$$

where the constant of proportionality is the inverse of the quantum of magnetic flux. Moreover, recalling the relation among current and voltage, $di_s/dt = V/L_J$, the definition of the Josephson inductance follows:

$$L_J = \frac{\Phi_0}{2\pi i_c \cos(\phi)}. \tag{4.13}$$

It is possible to approximate the dynamics of a Josephson junction via the *Resistively and Capacitively Shunted Junction (RCSJ) model*, which includes an ohmic resistance R and a capacity C arising from the geometry of the junctions itself:

$$i = i_1 \sin(\phi) + V/R + C dV/dt, \tag{4.14}$$

where i is the bias current circulating in the RCSJ circuit.

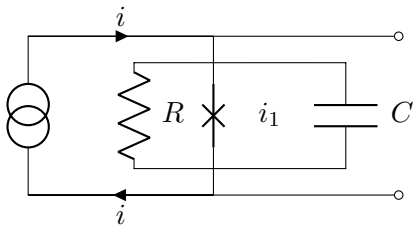

Figure 4.1: Diagram of RCSJ model.

From Josephson's voltage-phase relationship, it is possible to rewrite:

$$\frac{1}{\omega_J^2}\frac{d^2\phi}{dt^2} + \frac{1}{\omega_c}\frac{d\phi}{dt} = j - \sin(\phi), \tag{4.15}$$

where $j = i/i_1$ is the normalized supercurrent, $\omega_c = 2eR/\hbar$ is a characteristic frequency and $\omega_J = (2e/\hbar C)^{1/2}$ is the Josephson frequency. This is the equation of a damped nonlinear LC oscillator, therefore ω_J can be interpreted as the frequency of the oscillator in the small-amplitude limit while ω_c accounts for the energy dissipation due to the finite resistance R.

4.2 SQUID

A superconducting ring interrupted by two Josephson junctions constitutes the device called DC-SQUID (*Superconducting Quantum Interference Device*, [24]): a time-averaged direct voltage which is a periodic function of the flux is established across the two weak links by a direct bias current. Assuming that the two junctions are equal ($R_1 = R_2$; $C_1 = C_2$) and in particular that the two critical currents are the same $i_c \equiv i_{c1} = i_{c2}$, the current circulating around the loop is:

$$j = \frac{i_1 - i_2}{2} = i_c \cos\left(\frac{\phi_1 + \phi_2}{2}\right) \sin\left(\frac{\phi_1 - \phi_2}{2}\right) = -i_c \cos(\phi_+) \sin(\phi_-) \tag{4.16}$$

and the total transport current through the DC-SQUID is:

$$I = i_1 + i_2 = 2i_c \cos(\phi_-) \sin(\phi_+), \tag{4.17}$$

where the flux quantisation condition now reads $\phi_- = \pi(\Phi/\Phi_0) + n\pi$.
The self-inductance L_r of the SC ring generates a contribution to the total flux: $\Phi = \Phi_{ext} + L_r j$. Defining the screening parameter as $\beta = (2L_r j)/(\Phi_0)$ it is possible to rewrite the flux relation as:

$$\frac{\Phi}{\Phi_0} = \frac{\Phi_{ext}}{\Phi_0} - \frac{\beta}{2}\cos(\phi_+)\sin(\phi_-) \tag{4.18}$$

so that when $L_r \simeq 0$, $\beta \simeq 0$ and $\Phi \simeq \Phi_{ext}$, therefore the maximum transport current of the device is:

$$I_{max}(\Phi_{ext}) = 2I_c |\cos(\pi\, \Phi_{ext}/\Phi_0)| \tag{4.19}$$

and the DC-SQUID can be considered as a single Josephson Junction with critical current periodic in Φ_{ext} and therefore with tunable minimum self-inductance:

$$L_{s,min}(\Phi_{ext}) = \frac{\Phi_0}{2\pi I_{max}} = \frac{\Phi_0}{4\pi i_c |\cos(\pi\,\Phi_{ext}/\Phi_0)|}. \tag{4.20}$$

4.3 Flux-driven JPA

A *Josephson Parametric Amplifier* (*JPA*) consists of a *coplanar waveguide* (*CPW*) short-circuited to ground by a dc-SQUID, which is driven by an external time-dependent magnetic flux. The CPW is made of superconducting materials and it acts like a quasi one-dimensional, lossless transmission line with characteristic impedance $Z = \sqrt{L_0/C_0}$, L_0 and C_0 being the inductance and capacitance per unit length respectively. Since the lateral dimension should be of the order of the wavelength corresponding to the frequency range of the waves propagating in it, to the GHz regime corresponds a lateral dimension of a few millimeters and the CPW can be properly described with a distributed element model (a string of superconducting, infinitesimally small LC resonators) as shown in figure 4.2. The boundary conditions, a line break to the left and a short-circuit to ground to the right, make the CPW to behave like a *quarter-wavelength (λ/4-) resonator* whose fundamental frequency is $f = c \cdot (4d\sqrt{\varepsilon_{eff}})^{-1} = (4d\sqrt{L_0C_0})^{-1}$, where d is the length of the resonator and c is the speed of light in vacuum. The SQUID at the right end of the line contributes to the total resonance frequency of the JPA behaving like a flux-tunable, nonlinear inductor.

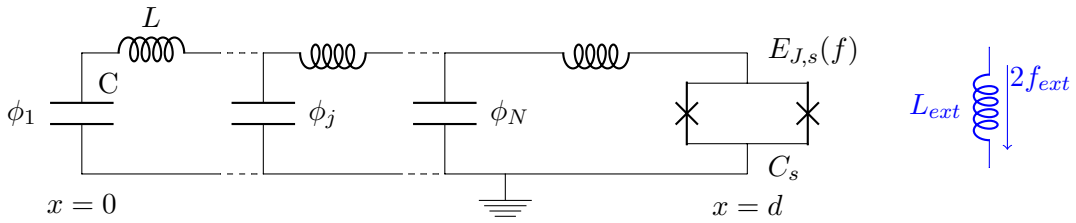

Figure 4.2: Equivalent circuit for the JPA.

For simplicity, the SQUID is modelled as symmetric, i.e. the two Josephson junctions are identical and have the same capacity $C_1 = C_2 = C_J$ and energy $E_1 = E_2 = E_J$ and the geometric inductance L_{SQ} can be considered as if separated in two equal parts $L_{SQ}/2$ with phase drop $f(t)$ over each one, driven through the mutual inductance M by an inductor L_{ext} of total phase $2f_{ext}$. Let the superconducting phases of the two Josephson junctions be $\phi_{J,i} = \phi_d \pm f$ where $\phi_d = \phi(d,t)$ is the phase of the CPW at $x = d$, so that the total phase drop over the SQUID is $(\phi_1 - \phi_2)/2 = \pi\Phi 2e/h = f$ (where flux quantization condition has been applied) and the magnetic flux through it is $\Phi = 2f\hbar/(2e)$. Then, the Lagrangian of the SQUID can be written with respect to the capacitive energy of a Josephson junction $E_{C,J} = \frac{(2e)^2}{2C_J}$ and the inductive energy of the SQUID loop $E_{L,SQ} = \left(\frac{\hbar}{2e}\right)^2 \frac{1}{2L_{SQ}}$ as [25]:

$$\mathcal{L}_{SQ} = \frac{\hbar^2}{2E_{C,J}}\dot{\phi_d}^2 + 2E_J\cos(\phi_d)\cos(f) + \frac{\hbar^2}{2E_{C,J}}\dot{f}^2 - E_{L,SQ}\left(4f^2 + 8\frac{M}{L_{ext}}f f_{ext}\right). \tag{4.21}$$

The Lagrangian for the superconducting phase field $\phi = \phi(x,t)$ across the bare λ/4-resonator , in the continuous limit, is [26]:

$$\mathcal{L}_r = \frac{dE_{L,r}}{2v^2}\int_0^d dx(\dot{\phi}^2 - v^2\phi'^2), \tag{4.22}$$

where $E_{L,r} = \hbar^2/(L_0 d(2e)^2)$ is the inductive energy of the CPW and $v = d/\sqrt{LC} = 1/\sqrt{L_0C_0}$ is the speed of the electromagnetic waves propagating in it.

The Euler-Lagrange equations of motion for $\phi_d(t)$ and $f(t)$ are obtained from the total Lagrangian of the system $\mathcal{L} = \mathcal{L}_{SQ} + \mathcal{L}_r$:

$$\begin{cases} \frac{\hbar^2}{E_c}\ddot{\phi_d} + 2E_J\cos(f)\sin(\phi_d) + E_{L,r}d\phi_d' = 0 & \text{(I)}; \\ \frac{\hbar^2}{2E_c}\ddot{f} + E_J\sin(f)\cos(\phi_d) + 4E_{L,SQ}(f + Mf_{ext}/L_{ext}) = 0 & \text{(II)}. \end{cases} \tag{4.23}$$

If the condition $\phi_d << 1$ is fulfilled, then $\cos(\phi_d) \simeq 1$ and the equation for f decouples from that for ϕ_d. When the external force is in the form of a constant equilibrium shift plus a small time-dependent oscillation, $f_{ext}(t) = F_{ext} + \delta f_{ext}\cos(\omega_p t)$ with $\delta f_{ext} << 1$, the SQUID response can be expressed as well in the form $f(t) = F + \delta f(t)$ with $\delta f(t) << 1$ and substituting in equation (4.23, II) leads to the equation of an harmonic oscillator driven by the external force $\delta f_{ext}(t)$:

$$\frac{\hbar^2}{2E_c}\delta\ddot{f}(t) + (E_J\cos(F) + 4E_{L,SQ})\delta f(t) = -\frac{4E_{L,SQ}M}{L_{ext}}\delta f_{ext}(t). \tag{4.24}$$

Therefore, the stationary response to the small external oscillation is itself an harmonic oscillation, $\delta f(t) = \delta f\cos(\omega_p t)$, with the same frequency as the external pump and amplitude:

$$\delta f = -\frac{8E_{L,SQ}ME_c/\hbar^2 L_{ext}}{\omega_f^2 - \omega_p^2}\delta f_{ext}, \tag{4.25}$$

where $\omega_f = \omega_J\sqrt{\cos(F) + 4E_{L,SQ}/E_J}$ is the frequency of the f-oscillator, $\omega_J = \sqrt{2E_J E_{C,J}}/\hbar$ is the Josephson plasma frequency. The solutions of the equation of motion for the bare CPW oscillator, $\ddot{\phi}^2 - v^2\phi'' = 0$, together with the boundary condition $\phi_0' = 0$ at its open end, are the eigen-modes $\phi_n(x,t) = \phi_1 e^{\pm ik_n t}\cos(k_n x)$ of eigen-frequencies $\omega_n = vk_n$. By substituting such solutions into equation (4.23, I):

$$(k_n d)\tan(k_n d) = \frac{2E_J\cos(F + \delta f(t))}{E_{L,r}} - \frac{2C_J}{C_0 d}(k_n d)^2. \tag{4.26}$$

When $\delta f(t) = 0$, since usually $C_J << C_0$ the second term on the right side of equation (4.26) can be omitted and solutions can be found graphically (figure 4.3, $\gamma = E_{L,r}/(2E_J\cos(F)) = 1/25$, $C_J = 0$ in solid line and $C = 2C_J/(C_0 d) = 0.05$ in dashed line in (a) and cavity spectrum $k_n d$ vs $1/\gamma$ in (b)).

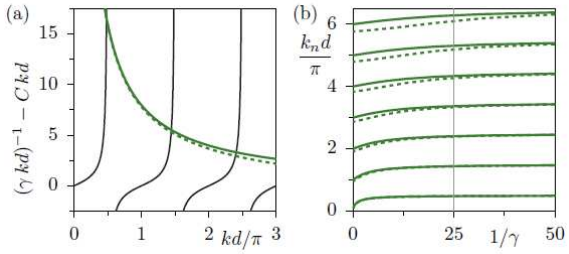

Figure 4.3: Graphic solution to equation (4.26), [26].

In particular, the fundamental mode is such that $k_0 d \simeq \pi/2$, hence $\omega_0/\omega_r \simeq 1$, where $\omega_0 = vk_0$ and ω_r is the fundamental frequency of the $\lambda/4$-resonator, and the tangent can be approximated by the first term in its Laurent series around $\pi/2$:

$$\tan(z) = \frac{1 - 1/2(z - \pi/2)^2 + o((z - \pi/2)^2)}{-(z - \pi/2) + o(z - \pi/2)} = -\frac{1}{z - \pi/2} + o\left(z - \frac{\pi}{2}\right)^2. \tag{4.27}$$

When a small modulation is present, $\delta f(t) << 1$, it is still possible to consider $\omega_0/\omega_r \simeq 1$ at first order in δf and hence a simple relation follows:

$$\omega_0 = \omega_r\frac{2E_J\cos(F + \delta f(t))}{2E_J\cos(F + \delta f(t)) + E_{L,r}}. \tag{4.28}$$

Since typically the inductive energy of the CPW is much smaller than the Josephson energy of the two junctions, $E_{L,r} << E_J$, it can be ignored. Finally, at first order in δf, $2E_J\cos(F+\delta f(t)) \simeq 2E_J\cos(F) - 2E_J\sin(F)\delta f\cos(\omega_p t) \simeq 2E_J cos(F)$ and to the first order in $\varepsilon/2 = -\tan(F)\delta f << 1$:

$$\omega_0 = \omega_r[1+\varepsilon/2\cos(\omega_p t)] \quad \Longrightarrow \quad \omega_0^2 = \omega_r^2[1+\varepsilon\cos(\omega_p t)]. \tag{4.29}$$

In the end, close to resonance the JPA behaves like a LC-oscillator with nonlinear, flux-tunable $L_r(\Phi) = L_0 + L_{SQ}$ and resonance frequency ω_0 modulated by the external ac-flux (figure 4.4 (a)).

4.4 Phase-sensitive gain

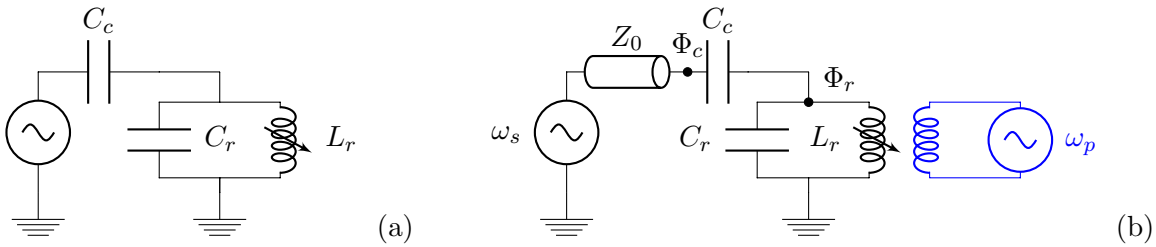

Figure 4.4: Circuit diagrams of a non-linear LC oscillator (a) and a phase sensitive parametric amplifier (b).

When the system is driven by an ac-flux in the regime of small pump amplitude at frequency $\omega_p \simeq 2\omega_0$, small probe signal at the resonator frequency are amplified. In the case of degenerate pumping $\omega_p = 2\omega_0$, it operates as a *phase sensitive parametric amplifier* [27]. With reference to figure 4.4 (b), the system is made up of a JPA resonator capacitively coupled (C_c) to a probe line of impedance Z_0 and can be described in terms of the canonical flux at each node $\Phi_i = \int_{-\infty}^{t} V_i dt'$, where V_i denotes the i-th node voltage with respect to ground. Due to the small dimension of the CPW, the canonical fluxes can be considered one-dimensional. At node r, Kirchoff's law yields:

$$C_c\left(\frac{d^2\Phi_r}{dt^2} - \frac{d^2\Phi_c}{dt^2}\right) = -C_r\frac{d^2\Phi_r}{dt^2} - \frac{1}{L_r}\Phi_r \Longrightarrow \frac{d^2\Phi_r}{dt^2} + \frac{1}{L_r(C_c+C_r)}\Phi_r = \frac{C_c}{C_c+C_r}\frac{d^2\Phi_c}{dt^2} \tag{4.30}$$

and, being $\omega_r = 1/\sqrt{L_r(C_c+C_r)}$ the resonant frequency and $k = C_c/(C_c+C_r)$ the coupling parameter, the equation can be rewritten as:

$$\frac{d^2\Phi_r}{dt^2} + \omega_r^2\Phi_r = k\frac{d^2\Phi_c}{dt^2}. \tag{4.31}$$

Including the parametric ac-pumping of strength ε and frequency ω_p (equation (4.29)) and assuming that k is kept constant, the equation for the r-node becomes:

$$\frac{d^2\Phi_r}{dt^2} + \omega_r^2[1+\varepsilon\cos(\omega_p t+\phi)]\Phi_r = k\frac{d^2\Phi_c}{dt^2}. \tag{4.32}$$

Such non-linear differential equation can be solved by making the following *ansatz* (for $i = \{c, r\}$):

$$\Phi_i = q_{i,1}\cos(\omega_p t/2t) - q_{i,2}\sin(\omega_p t/2) \quad \text{or equivalently} \quad \Phi_i = \frac{u_i}{2}\cos\left(\frac{\omega_p}{2}t\right) + \frac{u_i^*}{2}\sin\left(\frac{\omega_p}{2}t\right), \tag{4.33}$$

where the complex quadrature is defined as $u = q_1 + iq_2$. Substituting this *ansatz* in equation (4.32) and keeping only the slow-varying terms, i.e. the terms proportional to $\exp(i\omega_p t/2)$, yields to:

$$\left[\omega_r^2 - \left(\frac{\omega_p}{2}\right)^2\right]u_r + k\left(\frac{\omega_p}{2}\right)^2 u_c + \frac{\varepsilon}{2}u_r^* e^{i\phi} = 0. \tag{4.34}$$

At node c, the field takes the form:

$$\Phi_c(t) = \Phi_{in}(x/v_{ph} + t) + \Phi_{out}(-x/v_{ph} + t), \tag{4.35}$$

with $v_{ph} = 1/\sqrt{LC}$ the speed of the electromagnetic radiation in the line. Applying again Kirchoff's law:

$$C_c\left(\frac{d^2\Phi_c}{dt^2} - \frac{d^2\Phi_r}{dt^2}\right) = -\frac{1}{Z_0}\frac{d\Phi_c}{dt} + \frac{2}{Z_0}\frac{d\Phi_{in}}{dt}, \tag{4.36}$$

where $Z_0 = \sqrt{L/C}$ is the characteristic impedance of the transmission line. It is possible to substitute the *ansatz* (4.33) in equation (4.36) and again keeping only the slow-varying terms:

$$-C_c\left(\frac{\omega_p}{2}\right)^2(u_c - u_r) + \frac{i}{Z_0}\frac{\omega_p}{2}(u_c - 2u_{in}) = 0. \tag{4.37}$$

Finally, deriving with respect to position x and time t equation (4.35) it is possible to obtain the boundary condition:

$$-\frac{1}{L}\frac{\partial\Phi_c}{\partial x}\Big|_{x=0} = \frac{1}{Z_0}\left(\frac{\partial\Phi_c}{\partial t} - 2\frac{\partial\Phi_{in}}{\partial t}\right)\Big|_{x=0} \tag{4.38}$$

and again substituting the *ansatz* (4.33):

$$\frac{1}{Lv_{ph}}(u_{in} - u_{out}) - \frac{1}{Z_0}(u_c - 2u_{in}) = 0. \tag{4.39}$$

Using the expression for the output complex quadrature, $u_{out} = Z_0/(Z_L - Z_0)u_r + (Z_L - Z_0)/(Z_L + Z_0)u_{in}$, equations (4.34), (4.36), (4.39) can be solved with respect to u_{out} with appropriate approximations: first of all, let assume that at resonance $Z_0 << Z_L$. Then, being $Q = (C_c + C_r)/(Z_0C_c^2\omega_r)$, in the limit for $kQ = |Z_L(\omega_r)|/Z_0 = 1/(Z_0C_c\omega_r) >> 1$ the gain in the degenerate mode $\omega_p = 2\omega_r$ is:

$$g = \frac{q_{1,out} + iq_{2,out}}{\Phi_{in}} = 1 - 2\frac{1 + \gamma'\sin(\Delta\theta) - i\gamma'\cos(\Delta\theta)}{1 - \gamma'^2}, \tag{4.40}$$

where $\Delta\theta = 2\phi - \theta_p$, θ_p is the phase of the pump and $\gamma' = \varepsilon Q/(\omega_p\omega_r) = \varepsilon/(2\Gamma\omega_p)$, $\Gamma = \omega_r/(2Q)$

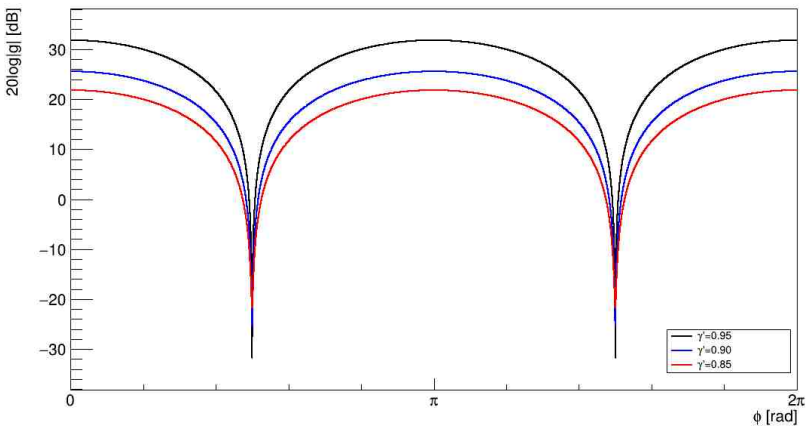

Figure 4.5: Voltage gain $20\log|g|$ of equation 4.40 in dB, for three different values of γ'.

In figure 4.5 it is plotted the voltage gain (in dB) with respect to the phase ϕ, when the pump phase is $\theta_p = 0$. It shows clearly that the flux-driven JPA has a phase sensitive gain: the signal is de-amplified for $\phi = \pi/2$ and amplified by about the same amount for $\phi = \pi$. Because of this feature, the JPA's are used at the HAYSTAC experiment in order to generate squeezed states of light (see section 3.2).

4.5 The pumpistor model

A qualitative description of the parametric effects of a flux-pumped SQUID is given, under suitably small-signal limits, by a linearized model: the system is reduced to a parallel combination of

a Josephson inductance and an additional circuit element, the *pumpistor* ([28], [29]), i.e. a complex frequency-dependent inductance which can periodically act as a negative resistance and provide parametric gain in the circuit.
As already seen in equation (4.16), the SQUID current can be expressed as the multiplication of a flux term and a phase term:

$$j(t) = 2I_c \cos(\pi\Phi_{ext}/\Phi_0) \times \sin(\phi) \tag{4.41}$$

the SQUID phase being $\phi = (\phi_1 - \phi_2)/2$. Assuming that the external flux is $\Phi_{ext} = \Phi_{dc} + \Phi_{ac}\cos(\omega_p t + \theta_p)$, $\Phi_{ac} <<$, it is possible to expand the current term with respect to the normalized flux amplitudes $F = \pi\Phi_{dc}/\Phi_0$ and $\delta f = \pi\Phi_{ac}/\Phi_0$:

$$2I_c \cos(\pi\Phi_{ext}/\Phi_0) \simeq 2I_c[\cos(F) - \sin(F)\delta f \cos(\omega_p t + \theta_p)]. \tag{4.42}$$

Regarding the phase, in the linear limit it can be expressed as a linear combination of the signal frequency, the pump frequency and an idler tone $\omega_i = \omega_s - \omega_p$ arising from the frequency mixing caused by the non-linear behaviour of the whole system. In the three-wave degenerate case, $\omega_s = \omega_i = \omega_p/2$; retaining only the terms proportional to the signal frequency, the phase term in equation (4.42) can be simplified to:

$$\sin[\phi(t)] \simeq \phi(t) = \tilde{\phi_s}\cos(\omega_s t + \theta_s) = (\tilde{\phi_s}/2)e^{-i\omega_s t}e^{-i\theta_s} + (\tilde{\phi_s}^*/2)e^{i\omega_s t}e^{i\theta_s}. \tag{4.43}$$

After substituting equation (4.43) into equation (4.16) and confronting it with the expression for a general oscillating current, $j = I_c e^{i\omega_s t} + T_c^* e^{-i\omega_s t} = j_+(t) + j_-(t)$, the component proportional to $e^{i\omega_s t}$ is:

$$j(t)_+ = I_c\tilde{\phi_s}[e^{-i\theta_s}\cos(F) - \sin(F)(\delta f/2)e^{i(\theta_p - \theta_s)}]e^{i\omega_s t}. \tag{4.44}$$

Analogously, the signal voltage term proportional to $e^{i\omega_s t}$ is:

$$V_s(t)_+ = \frac{1}{2}V_s e^{i\omega_s t} = \frac{\Phi_0}{2\pi}\frac{d}{dt}\left[\frac{1}{2}\tilde{\phi_s}e^{i\omega_s\theta_s}e^{i\theta_s}\right] = \frac{1}{2}\left[\frac{\Phi_0}{2\pi}\tilde{\phi_s}\omega_s(ie^{i\theta_s})\right]e^{i\omega_s t}. \tag{4.45}$$

Therefore, it is possible to define a signal admittance:

$$Y(\omega_s) = j_s(t)_+/V_s(t)_+ = (i\omega_s L_J)^{-1} + (i\omega_s L_p)^{-1}, \tag{4.46}$$

where L_J is the inductance of a single Josephson junction (equation (4.13)) and L_p is the phase-dependent inductance of the pumpistor:

$$L_1 = -L_J\frac{2}{\tan(F)}\frac{1}{\delta f}e^{i\Delta\theta}. \tag{4.47}$$

In particular, when $\Delta\theta = 2\theta_s - \theta_p = 0$ or $\Delta\theta = \pi$ the pumpistor acts as a negative or a positive inductance respectively. At $\Delta\theta = \pi/2$ the inductance L_p becomes imaginary, hence contributes to the impendance as a positive resistance dissipating energy, whereas at $\Delta\theta = 3\pi/2$ it contributes as a negative resistance. In this last state, the pumpistor extracts power from the pump and injects it into the circuit at the signal frequency, providing gain. This behaviour is illustrated in figure 4.6.

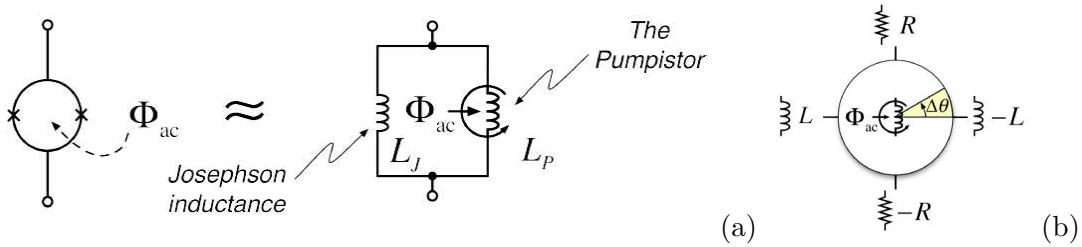

Figure 4.6: a)SQUID equivalent to an inductance+pumpistor system; b)phase-dependence of L_1, [28].

Chapter 5

The HAYSTAC experiment

The *Haloscope at Yale Sensitive to Axion Cold dark matter (HAYSTAC)* experiment [22] is designed to probe the $m_a > 10\ \mu eV/c^2$ mass range for QCD axions, assuming that they saturate the cosmological dark matter density. The previous haloscope has been enhanced by introducing a *squeezed-state receiver (SSR)* in order to squeeze under the quantum limit one quadrature of the vacuum noise incident on the cavity. This quantum system improves the maximum QCD axion visibility bandwidth and as a consequence it increases the scan rate R (see equation (3.13)).

5.1 SSR experimental setup

The SSR experimental setup is shown in figure 5.1. The SQ, the cavity and the AMP sit in a dilution refrigerator with base temperature of 20 mK. The cavity has volume V_c=1.5 liters, unloaded quality factor $Q_0 = 47000 \pm 5000$ and it is embedded in a region of high static magnetic field generated by an 8-T solenoid magnet. The cavity is tuned by a rotating off-axis tuning rod. The two JPAs are held above the cavity in a shielding can to reduce the magnetic flux through each of the SQUID loops to much less than one magnetic flux quantum. The pump tone is delivered to each JPA through directional couplers, passive devices which couple 10-dB of power flowing in one direction in the transmission line to the JPA's pump port. Each JPA is connected via superconducting cables that minimize transmission losses to an ensamble of four microwave circulators that route signals non-reciprocally in order to create insulation between the SSR's elements and realize the time sequence of operations (vacuum state squeezing in the SQ, possible displacement by a QCD axion field in the cavity, unsqueezing in the AMP, further amplification and detection). On the SQ pump's input line a voltage-controlled variable attenuator and a phase shifter allow to control both the amplitude and phase of the SQ pump.
At the chain input, a switch allows to inject either a probe tone from a *Vector Network Analyzer* or Johnson-Nyquist vacuum noise sourced from a 50 Ω at 300 K. At the output, other two double-junction circulators insulate the AMP from signals reflected from a *High Electron Mobility Transistor (HEMT)* amplifier which follows held at 4K.
At the output of the HEMT a 6-dB directional coupler extracts a portion of the output signal and leads it to to the VNA, which is used to measure the coupling rates k_m and $k_l + k_a$. The other portion of the signal is injected in the IQ mixer's rf port.
The QCD axion signal is modelled as a microwave generator (AWG) at room temperature coupled to the cavity at rate k_a. The frequency of the axion-induced oscillating field $\mathbf{E}$ is expected to fall within the bandwidth of a transverse magnetic TM_{0n0}-like mode of the cavity. A second microwave generator drives both JPAs and serves as a local oscillator (LO) for the in-phase and quadrature (IQ) mixer. The signal has amplitude A and frequency ω_0:

$$A\sin(\omega_0 t + \phi) = A\sin(\omega_0 t)\cos(\phi) + A\cos(\omega_0 t)\sin(\phi) = I(\phi)\cos(\omega_0 t) + Q(\phi)\sin(\omega_0 t) \tag{5.1}$$

where $I(\phi) = A\sin(\phi)$ and $Q(\phi) = A\cos(\phi)$ are the two quadrature amplitudes. It is mixed together with a local oscillator (LO) $\cos(\omega_0 t + \phi_{LO})$ with the same frequency as the signal (*homodyne detection*) and phases $\phi_{LO} = 0$ at the I input and $\phi_{LO} = -\pi/2$ at the Q input; the mixed signal is then low-pass filtered to cut the high-frequency terms and to extract the two quadratures:

$$A\sin(\omega_0 t + \phi)\sin(\omega_0 t) = \frac{A}{2}[1 - \cos(2\omega_0 t)]\cos(\phi) + \frac{A}{2}\sin(2\omega_0 t)\sin(\phi) \longrightarrow \frac{Q(\phi)}{2}; \tag{5.2}$$

$$A\sin(\omega_0 t + \phi)\cos(\omega_0 t) = \frac{A}{2}[\cos(2\omega_0 t) - 1]\sin(\phi) + \frac{A}{2}\sin(2\omega_0 t)\cos(\phi) \longrightarrow -\frac{I(\phi)}{2}. \tag{5.3}$$

A frequency divider converts the pump frequency ω_p to the resonance frequency of both JPAs, ω_0 at the input of the IQ mixer.
The in-phase and quadrature signals, previously mixed down, are amplified and reache an *analogue-to-digital converter* where they are digitized.

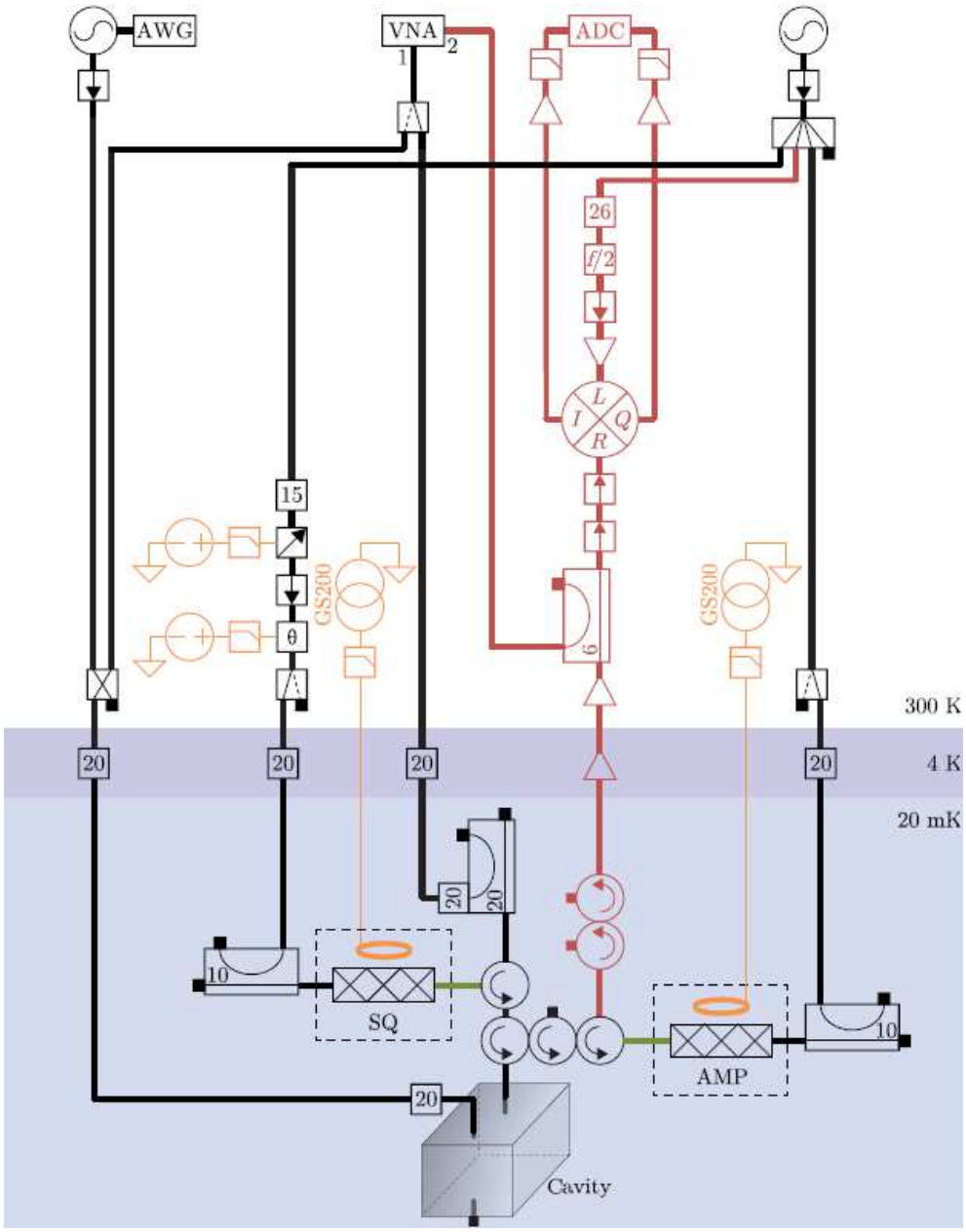

Figure 5.1: Schematic of the SSR. [22]

5.2 Experimental results

The HAYSTAC experiment was able to measure an off-resonance vacuum squeezing, defined as the ratio between the SQ-on and the SQ-off variance of the squeezed quadrature at the system output, of

$$S = \frac{\sigma_{on}^2}{\sigma_{off}^2} = 0.4 \quad \text{or equivalently} \quad -10log_{10}S = 4 \text{ dB} \tag{5.4}$$

yielding a scan rate enhancement of a factor 1.9. In figure 5.2, the experimental voltage fluctuation V_X histogram of the squeezed quadrature X_1 with respect to the angle θ between the squeezer and the amplifier, with the SQ off (a) and with the SQ on (b) are compared [1].

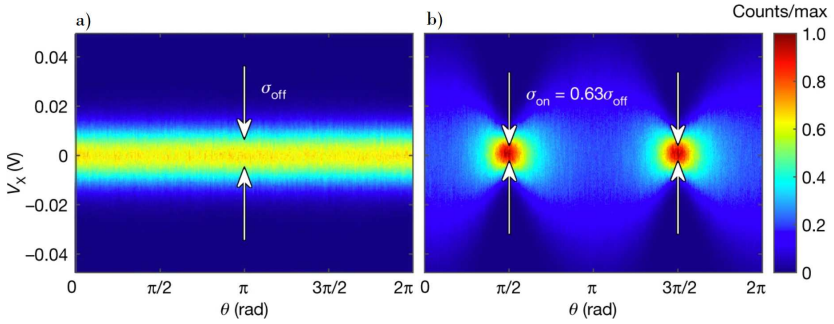

Figure 5.2: Experimental voltage fluctuations of the squeezed quadrature X_1, [1].

Despite the theoretical prevision of a deliverable squeezing up to 30 dB (see equation (4.40) and figure 4.5), in practice squeezing is limited by the transmissivity $\eta \simeq 0.63$ of the cables and microwave components in the SSR system. Such losses can be described quantitatively with a beam splitter model as shown in figure 5.3 [20]: the input squeezed state is transmitted with coefficient η while the input at the vacuum port is transmitted with coefficient $\epsilon = 1 - \eta$.

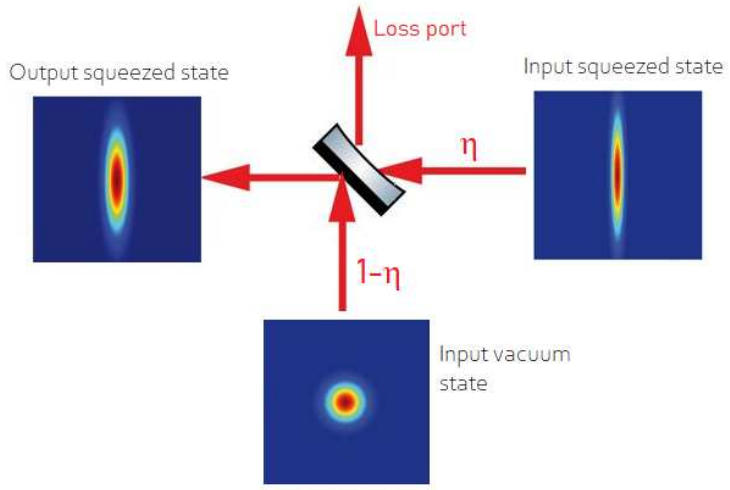

Figure 5.3: Beam splitter model of system losses and squeezed state degradation.

As a result, recalling that the vacuum state is a coherent state with variance $\sigma_{vac}^2 = 1$ (see equation (3.8)), the deliverable squeezing at the output of the SSR has the following expression [1] (see figure 5.4):

$$\sigma_{out}^2 = \eta\sigma_{in}^2 + (1-\eta)\sigma_{vac}^2 \Longrightarrow S_{out} = \eta S_{in} + (1-\eta) \tag{5.5}$$

To sum up, in consequence of the losses the squeezed state and the vacuum state add and the output is still a squeezed state with a reduced degree of squeezing.

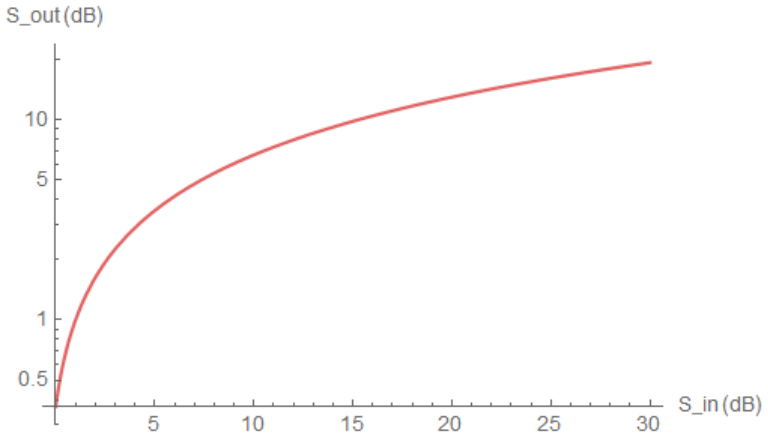

Figure 5.4: Plot of S_{out} with respect to the input S_{in}, with $\eta = 0.63$ (equation (5.5)).

The SSR system has been used to probe over 70 MHz of the parameter space in the 4.100-4.178 GHz window (skipping the 4.140-4.145 GHz range corresponding to a transverse electric mode which does not couple to the axion) in half the time that would have been required without squeezing. No evidence of dark matter has been found within the QCD axion mass ranges 16.96-17.12 $\mu eV/c^2$ and 17.14-17.28 $\mu eV/c^2$. Finally, the HAYSTAC experiment excludes QCD axions with coupling constant $g_\gamma \geq g_\gamma^{KSVZ}$ at the 90% level.

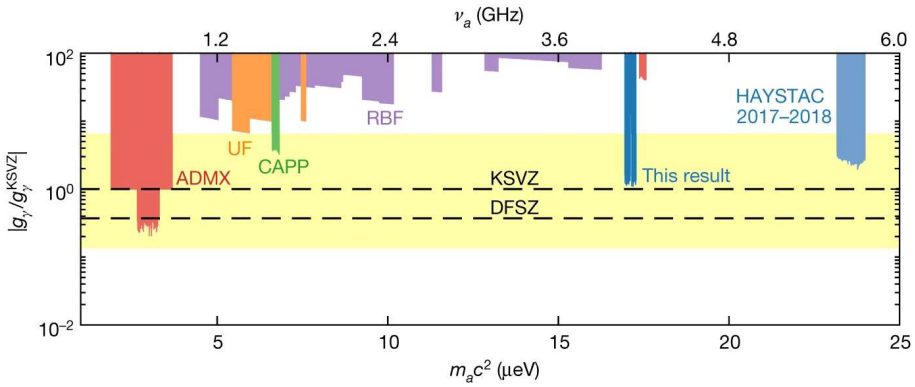

Figure 5.5: Exclusion results from ADMX, UF, CAPP (*Center for Axion and Precision Physics research*) and RBF collaboration, together with the HAYSTAC previous (2017-2018) and current results. The yellow band represents the most natural KSVZ and DFSZ models for QCD axion, the specific KSVZ and DFSZ model lines are shown as black dashed lines, [1].

Chapter 6

Conclusions

The QCD axion may provide a solution to the strong-CP problem of quantum chromodynamics and the unknown nature of dark matter, therefore explaining why the interest in carrying out experiments in order to search for it increased in recent years. The haloscope technique, based on the interaction of the axion field with the electromagnetic radiation in a resonant cavity, has provided the most sensitive experimental approach so far, but it happens to be sorely limited, even at sub-Kelvin system's temperatures, by the SQL prevailing over an expected signal of roughly $P_a \simeq 20^{-23}$ W. Furthermore, the time scale over which the cavity haloscopes are able to sweep out appreciable fractions of parameter space of the axion Compton frequency is unreasonably long.
These major experimental shortcomings can be circumvented by partially replacing the vacuum noise in the cavity with squeezed vacuum, in so doing enabling high sensitivity over a broader bandwidth and a more rapid search. Squeezed vacuum can be generated by a flux-driven JPA, basically a non-linear LC-resonator whose parametric behaviour comes from the two Josephson junctions comprising its inductance. Working in the degenerate mode, $\omega_0 \simeq \omega_p$, the JPA produces a phase-sensitive gain and squeezes one vacuum quadrature while amplifying the other one by the same amount and reaches in theory even more than 30 dB of deliverable squeezing (4.40).
In practice, the squeezed state in the cavity is contaminated by noise vacuum arising from the losses of cables and microwave components. The HAYSTAC experiment enhanced its detector by including a squeezed-state receiver system and reached an off-resonance vacuum squeezing of 4 dB with microwave transmission efficiency $\eta \simeq 0.63$. It managed to reduce the scan rate by a factor two with respect to a classical haloscope and put further limits on the QCD axion mass, excluding the ranges 16.96-17.12 $\mu eV/c^2$ and 17.14-17.28 $\mu eV/c^2$.
If microwave losses are reduced, a subquantum limited haloscope will reap larger benefits. For example, coupling the cavity to an auxiliary resonant circuit through simultaneous two-mode squeezing and state-swapping interactions should boost transmission efficiency above 90 % and increase scan rate up to 15-fold enhancement beyond the quantum limit [30].
To conclude, the interest in phase-sensitive amplification and JPAs extends to the field of quantum information processing: the quantum state of a superconducting bit can be encoded onto the strong output field of a frequency-tunable resonator, rendering a signal-to-noise ratio sufficient for single-shot state detection, a fundamental task for realizing a quantum computer [27]. Moreover, gravitational waves kilometer-size detectors use laser light to detect tiny lenght changes and are so sensitive that they are limited by quantum noise which overlaps gravitational-wave signals. Through squeezing, it is possible to change the noise properties and lower the quantum mechanical fluctuations to improve the sensitivity [31].

Bibliography

[1] K. M. Backes et al. "A quantum enhanced search for dark matter axions". In: *Nature* 590.7845 (Feb. 2021), pp. 238–242. DOI: 10.1038/s41586-021-03226-7.

[2] F. Chadha-Day, J. Ellis, and D. J. E. Marsh. "Axion dark matter: What is it and why now?" In: *Science Advances* 8.8 (2022), eabj3618. DOI: 10.1126/sciadv.abj3618.

[3] C. Abel et al. "Measurement of the Permanent Electric Dipole Moment of the Neutron". In: *Phys. Rev. Lett.* 124 (8 Feb. 2020), p. 081803. DOI: 10.1103/PhysRevLett.124.081803.

[4] R. D. Peccei and H. R. Quinn. "CP Conservation in the Presence of Pseudoparticles". In: *Physical Review Letters* 38 (1977), pp. 1440–1443.

[5] M. Gorghetto and G. Villadoro. "Topological susceptibility and QCD axion mass: QED and NNLO corrections". In: *Journal of High Energy Physics* 2019.3 (Mar. 2019). DOI: 10.1007/jhep03(2019)033.

[6] David J.E. Marsh. "Axion cosmology". In: *Physics Reports* 643 (July 2016), pp. 1–79. DOI: 10.1016/j.physrep.2016.06.005.

[7] F. Zwicky. "Die Rotverschiebung von extragalaktischen Nebeln. (German) [The red shift of extragalactic neubulae]". In: *Helvetica Physica Acta* 6 (Jan. 1933), pp. 110–127.

[8] R. W. Wilson and A. A. Penzias. "Isotropy of Cosmic Background Radiation at 4080 Megahertz". In: *Science* 156.3778 (1967), pp. 1100–1101. DOI: 10.1126/science.156.3778.1100.

[9] V. C. Rubin and Jr. Ford W. K. "Rotation of the Andromeda Nebula from a Spectroscopic Survey of Emission Regions". In: 159 (Feb. 1970), p. 379. DOI: 10.1086/150317.

[10] J. E. Kim. "Weak-Interaction Singlet and Strong CP Invariance". In: *Phys. Rev. Lett.* 43 (2 July 1979), pp. 103–107. DOI: 10.1103/PhysRevLett.43.103.

[11] M.A. Shifman, A.I. Vainshtein, and V.I. Zakharov. "Can confinement ensure natural CP invariance of strong interactions?" In: *Nuclear Physics B* 166.3 (1980), pp. 493–506. ISSN: 0550-3213. DOI: https://doi.org/10.1016/0550-3213(80)90209-6.

[12] A P Zhitnitskii. "Possible suppression of axion-hadron interactions". In: *Sov. J. Nucl. Phys. (Engl. Transl.); (United States)* 31:2 (Feb. 1980).

[13] M. Dine, W. Willy Fischler, and M. A. Srednicki. "A Simple Solution to the Strong CP Problem with a Harmless Axion". In: *Physics Letters B* 104 (1981), pp. 199–202.

[14] C. Bartram et al. "Axion dark matter experiment: Run 1B analysis details". In: *Phys. Rev. D* 103 (3 Feb. 2021), p. 032002. DOI: 10.1103/PhysRevD.103.032002.

[15] Y. K. Semertzidis and S. Youn. "Axion dark matter: How to see it?" In: *Science Advances* 8.8 (2022), eabm9928. DOI: 10.1126/sciadv.abm9928.

[16] P. Sikivie. "Experimental Tests of the Invisible Axion". In: *Phys. Rev. Lett.* 51 (16 Oct. 1983), pp. 1415–1417. DOI: 10.1103/PhysRevLett.51.1415.

[17] K. van Bibber, K. Lehnert, and A. Chou. "Putting the squeeze on axions". In: *Physics Today* 72.6 (2019), pp. 48–55. DOI: 10.1063/PT.3.4227.

[18] A. Papoulis. *Probability, random variables and stochastic processes*. English (US). 4th. McGraw-Hill, 2001.

[19] H. B. Callen and T. A. Welton. "Irreversibility and Generalized Noise". In: *Phys. Rev.* 83 (1 July 1951), pp. 34–40. DOI: 10.1103/PhysRev.83.34.

[20] H.A. Bachor and T. Ralph. "Squeezing experiments". In: *A Guide to Experiments in Quantum Optics*. John Wiley Sons, Ltd, 2004. Chap. 9, pp. 232–309.

[21] Sheon S Y Chua et al. “Quantum squeezed light in gravitational-wave detectors”. In: *Classical and Quantum Gravity* 31 (2014), p. 183001.

[22] M. Malnou et al. “Squeezed Vacuum Used to Accelerate the Search for a Weak Classical Signal”. In: *Phys. Rev. X* 9.17 (2 May 2019), p. 021023. DOI: 10.1103/PhysRevX.9.021023.

[23] J. Bardeen, L. N. Cooper, and J. R. Schrieffer. “Theory of Superconductivity”. In: *Phys. Rev.* 108 (5 Dec. 1957), pp. 1175–1204. DOI: 10.1103/PhysRev.108.1175.

[24] J.C. Gallop. *SQUIDs, the Josephson Effects and Superconducting Electronics*. Adam Hilger, 1991.

[25] M. Wallquist, V. S. Shumeiko, and G. Wendin. “Selective coupling of superconducting charge qubits mediated by a tunable stripline cavity”. In: *Phys. Rev. B* 74 (22 Dec. 2006), p. 224506. DOI: 10.1103/PhysRevB.74.224506.

[26] W. Wustmann and V. S. Shumeiko. “Parametric resonance in tunable superconducting cavities”. In: *Phys. Rev. B* 87 (18 May 2013), p. 184501. DOI: 10.1103/PhysRevB.87.184501.

[27] P. Krantz. “The Josephson parametric oscillator - From microscopic studies to single-shot qubit readout”. PhD thesis. 2016.

[28] K. Sundqvist et al. “The pumpistor: A linearized model of a flux-pumped superconducting quantum interference device for use as a negative-resistance parametric amplifier”. In: *Applied Physics Letters* 103 (Sept. 2013), pp. 2603–. DOI: 10.1063/1.4819881.

[29] K. Sundqvist and P. Delsing. “Negative-resistance models for parametrically flux-pumped superconducting quantum interference devices”. In: *EPJ Quantum Technology* 1 (6 July 2014). DOI: 10.1140/epjqt6.

[30] K. Wurtz et al. “Cavity Entanglement and State Swapping to Accelerate the Search for Axion Dark Matter”. In: *PRX Quantum* 2 (4 Dec. 2021), p. 040350. DOI: 10.1103/PRXQuantum.2.040350.

[31] F. Acernese et al. “Increasing the Astrophysical Reach of the Advanced Virgo Detector via the Application of Squeezed Vacuum States of Light”. In: *Phys. Rev. Lett.* 123 (23 Dec. 2019), p. 231108. DOI: 10.1103/PhysRevLett.123.231108.